The International Journal of Advanced Manufacturing Technology (2018) 97:2509–2527
https://doi.org/10.1007/s00170-018-2017-7

ORIGINAL ARTICLE

Milling stability prediction with simultaneously considering the multiple factors coupling effects—regenerative effect, mode coupling, and process damping

Yongjian Ji[1] · Xibin Wang[1] · Zhibing Liu[1] · Hongjun Wang[2] · Li Jiao[1] · Lu Zhang[1] · Tao Huang[1]

Received: 15 January 2018 / Accepted: 4 April 2018 / Published online: 16 May 2018

Abstract
Chatter is a kind of self-excited vibrations which is related to regenerative effect, mode coupling effect, and process damping, etc. To predict milling chatter more accurately, a suitable dynamical model of milling process which can reflect the practical chatter mechanism should be obtained firstly. In this paper, a new milling dynamical model which simultaneously considers the regenerative effect, mode coupling effect, and process damping is established. Based on the new dynamical model and the updated full-discretization method (FDM), the coupling influences of regenerative effect, mode coupling effect, and process damping on the accurate of the stability lobe diagrams (SLDs) for up-milling and down-milling operations are investigated. A series of numerical simulation and experiments are carried out to verify the accuracy of the proposed milling dynamical model. The experiment results show that the mode coupling effect and process damping have great influences on the prediction of milling stability. The SLD which obtained by the new milling dynamical equation (considering the regenerative effect, mode coupling, and process damping) is more accurate than that which obtained by only considering the regenerative effect.

Keywords Milling chatter prediction · Mode coupling effect · Regenerative effect · Process damping · Stability lobe diagrams

1 Introduction

Chatter is a kind of self-excited vibrations which always leads to poor workpiece surface quality. Stability prediction is one of the significant ways to avoid the machining chatter. A proper dynamical model which can reflect the machining process is the basic of chatter prediction. Regenerative effect [1] and mode coupling effect [2] are the two most used theories in explaining and predicting the self-excited vibrations (i.e., chatter). In addition, process damping [3] also has an influence which is not to be overlook on the accurate of milling stability prediction, especially at low speed cutting situation. Similarly, the multiple regenerative effects [4] and the loss-of-contact effects [5, 6] also influence the dynamic characteristic of cutting process.

As discussed by Quintana and Ciurana [7], regenerative effect is the most important cause of chatter. Most stability prediction methods, such as the frequency domain methods [8–10], the time domain methods [11–15], and the numerical integration methods [16–18], are based on the linear dynamical model which considering regenerative effect as the main cause of chatter and neglecting the mode coupling effect and process damping.

Balachandran et al. [5, 19] pointed out that although the linear dynamical models are helpful for predicting the onset of chatter, they are not helpful for determining the nature of the instability. For understanding the nature of the instability and post-instability motions, Balachandran and Zhao [20, 21] proposed the nonlinear dynamical model which taking the loss-

✉ Zhibing Liu
liuzhibing@bit.edu.cn

Yongjian Ji
jiyongjian@bit.edu.cn

[1] Key Laboratory of Fundamental Science for Advanced Machining, Beijing Institute of Technology, No.5 South Zhongguancun Street, Haidian District Beijing 100081, People's Republic of China

[2] Key Laboratory of Modern Measurement and Control Technology, Beijing Information Science and Technology University, No.12 East Qinghexiaoying Road, Beijing 100192, People's Republic of China

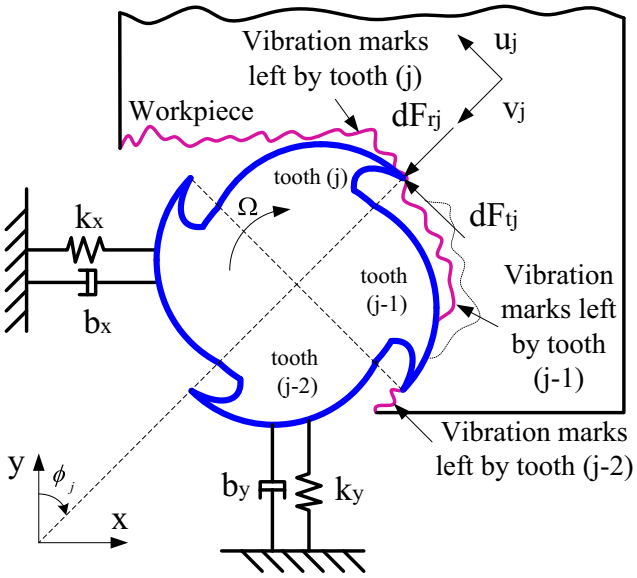

Fig. 1 Mechanical model of milling process (Source: Ref [7, 8])

of-contact non-linearities and multiple regenerative effects into account, the results show that the proposed nonlinear dynamical model is more accurate in the aspect of stability predictions for low-immersion operations. Also, they pointed out that the stability lobe diagrams for up-milling and down-milling operations are different from each other when the radial immersion ratio is changed, and the differences are believed to be due to the loss-of-contact effects that become prominent as the immersion ratio is reduced [20].

Zhang et al. [22] pointed out that in the actual milling process, the mode coupling, which the multiple degree-of-freedom system vibrates simultaneously in many directions with different amplitudes and phases, also has influences on the stability of machining process. Gasparetto [23] analyzed mode coupling chatter from the point-of-view of the system theory; in order to simplify the model and to focus on the analysis of chatter due to the mode coupling effect, damping was ignored in the dynamical model. Afterwards, Gasparetto [24] utilized eigenvalue analysis method to study mode coupling chatter, and some strategies for avoiding mode coupling chatter were proposed. Based on Gasparetto's [23] dynamical model, Trevisani et al. [25] proposed a more general dynamic model which taking damping phenomena into account, based on the proposed model; the model coupling phenomenon from a wood milling process was explored. Hoffmann and Gaul [26] investigated the relationship between the viscous structural damping and mode coupling instability without considering the regenerative effect. For the past few years, the mode coupling effect on robot machining and orthogonal metal cutting was also investigated by Pan et al. [27] and Iturrospe et al. [28], respectively.

Process damping is generated at the tool and workpiece interface due to the indentation of undulations under the flank face of the tool [29–31]; it has profound influence on the process stability at low cutting speed situation [32]. Huang and Wang [33] showed that plowing mechanism contributes more to the total damping effect than the shearing mechanism, and process damping decreases with increasing cutting velocity. Ahmadi and Ismail [34] explored the effect of nonlinear process damping on the stability lobes of turning operation. Later, Ahmadi and Ismail [32] studied the influence of process damping on milling stability lobes by multi-frequency and semi-discretization methods (SDM); it is shown that the SDM can provide more accurate results, and the experiment results indicated that the stability lobes which consider process damping closely agree with the cutting tests. Ahmadi [35] used a time-delayed system with nonlinear damping to describe the dynamics of chip formation.

The regenerative effect, mode coupling effect, and process damping are always separately considered in most of the existing researches to explain and predict the chatter phenomenon. Zhang et al. [22] explored the stability boundaries characteristics by simultaneously considering the structural mode coupling effect and regenerative effect; the results showed that the cross coupled terms have great influence on the stability boundary, the regenerative effect, and mode coupling effect co-exist in the practical milling situation, while, in Zhang's research, the process damping was ignored. Based on the

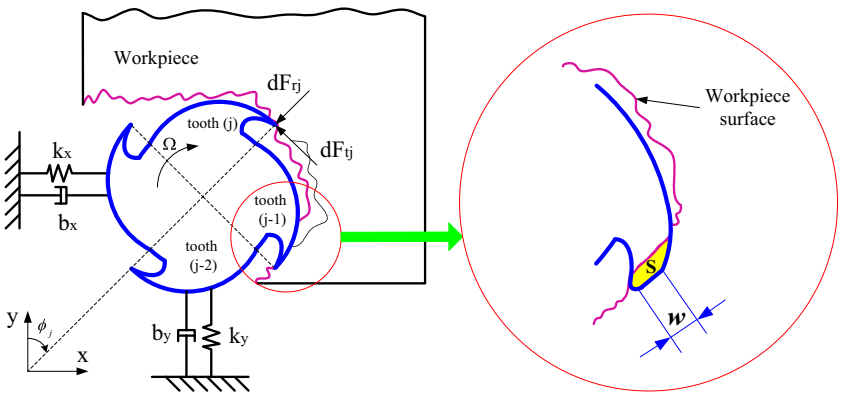

Fig. 2 The enlarged view for the indentation of undulations under the flank face of the cutter

mathematical model which considers regenerative effect, Malekian et al. [36] investigated the mechanistic modeling of micro-milling forces, which the effects of plowing, elastic recovery, run-out, and dynamics were taken into account. Li et al. [29] created an extended dynamic milling model including mode coupling and process damping to predict the stability and surface location error. Milling operation is a very complicated process; in practical milling case, chatter is usually caused by multiple factors rather than a single reason. If we want to predict the real milling situation, then comprehensive factors should be taken into account.

In this paper, we established a new linear milling dynamical model by simultaneously considering the regenerative effect, mode coupling effect, and process damping. In order to focus on the linear milling dynamical model resulting from the multiple factors coupling effects (i.e., the regenerative effect, mode coupling effect, and process damping), a simplified two-degree-of-freedom dynamical model is proposed. Based on the new dynamical model, the stability lobe diagrams (SLD) for up-milling and down-milling operations are obtained. The experiment results show that the SLD which obtained by the new milling dynamical equation (i.e., considering the regenerative effect, mode coupling, and process damping) is more accurate than that which obtained by only considering the regenerative effect.

The rest of the papers are shown as follows: Sect. 2 establishes the dynamical model of two-DOF milling system; in this section, the dynamical model of milling process which considers the regenerative effect, mode coupling effect, and process damping is established. Section 3 introduces the updated full-discretization method (FDM) for chatter stability prediction. The numerical simulation and experimental validation of the new milling dynamical model are shown in Sect. 4. The conclusions and future works are laid out in Sect. 5.

2 Model equation of two-DOF system

The milling system can be simplified as a vibration system which is described by springs and dampers in two perpendicular directions [37], which mean that the milling system can be regarded as a system which consists of modal mass, modal damping, and modal stiffness. In this paper, the tool is assumed to be flexible compared with the rigid workpiece; then, a linear milling dynamical model with two-DOF is proposed.

2.1 Dynamical model of milling process by considering regenerative effect and mode coupling effect

Regenerative effect is caused by the variation of chip thickness and cutting forces. As shown in Fig. 1, during milling process, the previous tooth vibrations leave a wavy on the surface of the workpiece, when the next tooth in cut, it will attack the wavy surface, leading to the variation of chip thickness and cutting forces, finally chatter occurs [7]. Here, the tool is assumed to be flexible compared with the rigid workpiece.

Mode coupling, which defined as the milling system vibrates with different amplitude and phases in different directions simultaneously, also exists in the milling process. The milling dynamical equation of two DOF which consider the mode coupling and regenerative effect can be described as the following matrix form [22].

$$\begin{bmatrix} m_x & m_{xy} \\ m_{yx} & m_y \end{bmatrix}\begin{bmatrix} \ddot{x}(t) \\ \ddot{y}(t) \end{bmatrix} + \begin{bmatrix} c_x & c_{xy} \\ c_{yx} & c_y \end{bmatrix}\begin{bmatrix} \dot{x}(t) \\ \dot{y}(t) \end{bmatrix} + \begin{bmatrix} k_x & k_{xy} \\ k_{yx} & k_y \end{bmatrix}\begin{bmatrix} x(t) \\ y(t) \end{bmatrix} = \begin{bmatrix} Fx(t) \\ Fy(t) \end{bmatrix} \tag{1}$$

where m, c, and k are the modal mass, modal damping, and modal stiffness, respectively. The subscript "x" means the response in the "x" direction is excited by the input from the "x" direction; The subscript "y" means the response in the "y" direction is excited by the input from the "y" direction; the subscript "xy" means the response in the "y" direction is excited by the input from the "x" direction; the subscript "yx" means the response in the "x" direction is excited by the input from the "y" direction. $F_x(t)$ and $F_y(t)$ are the cutting forces due to the tool rotation, as shown in the following equations [22]:

$$\begin{aligned} Fx(t) = &\sum_{j=1}^{N} \int_0^{ap} g(\phi j(t))(fj(t))(Ktc\cos\phi j(t) + Knc\sin\phi j(t))dz \\ &+ \sum_{j=1}^{N} \int_0^{ap} g(\phi j(t))(Kte\cos\phi j(t) + Kne\sin\phi j(t))dz \end{aligned} \tag{2}$$

$$\begin{aligned} Fy(t) = &\sum_{j=1}^{N} \int_0^{ap} g(\phi j(t))(fj(t))(-Ktc\sin\phi j(t) + Knc\cos\phi j(t))dz \\ &+ \sum_{j=1}^{N} \int_0^{ap} g(\phi j(t))(-Kte\sin\phi j(t) + Kne\cos\phi j(t))dz \end{aligned} \tag{3}$$

where K_{tc} and K_{nc} are the tangential and the normal cutting coefficients; K_{te} and K_{ne} are the tangential and the normal edge coefficients, respectively. a_p is the axial depth of cut.

$$\begin{aligned} fj(t) = &[fz + x(t-T) - x(t)]\sin(\phi j(t)) \\ &+ [y(t-T) - y(t)]\cos(\phi j(t)) \end{aligned} \tag{4}$$

$$\phi j(t) = \frac{2\pi\Omega}{60}t + (j-1)\frac{2\pi}{N} \tag{5}$$

$$g(\phi j(t)) = \begin{cases} 1 & if\ \phi st < \phi j(t) < \phi ex \\ 0 & otherwise \end{cases} \tag{6}$$

where f_z is the nominal feed per tooth and $T = 60/N\Omega$. Ω is the spindle speed in (rpm), N is the number of teeth. ϕst and ϕex are the start and exit angles of the jth cutter tooth. For down-

milling $\phi st = ar\cos(2ae/D-1)$ and $\phi ex = \pi$; for up-milling, $\phi st = 0$ and $\phi ex = \arccos(1-2ae/D)$, ae/D is the radial immersion ratio.

Substituting Eqs. (2) and (3) into Eq. (1), the following equation can be obtained.

$$\begin{bmatrix} m_x & m_{xy} \\ m_{yx} & m_y \end{bmatrix}\begin{bmatrix} \ddot{x}(t) \\ \ddot{y}(t) \end{bmatrix} + \begin{bmatrix} c_x & c_{xy} \\ c_{yx} & c_y \end{bmatrix}\begin{bmatrix} \dot{x}(t) \\ \dot{y}(t) \end{bmatrix} + \begin{bmatrix} k_x & k_{xy} \\ k_{yx} & k_y \end{bmatrix}\begin{bmatrix} x(t) \\ y(t) \end{bmatrix} = \begin{bmatrix} -a_p h_{xx} & -a_p h_{xy} \\ -a_p h_{yx} & -a_p h_{yy} \end{bmatrix}\begin{bmatrix} x(t) \\ y(t) \end{bmatrix} - \begin{bmatrix} -a_p h_{xx} & -a_p h_{xy} \\ -a_p h_{yx} & -a_p h_{yy} \end{bmatrix}\begin{bmatrix} x(t-T) \\ y(t-T) \end{bmatrix} + \mathbf{F}_0 \tag{7}$$

where $\mathbf{F}_0$ is the steady force excitation and it can be ignored since it is unrelated to the linear chatter stability, the details of $\mathbf{F}_0$ can be obtained in Ref [22]. h_{xx},h_{xy},h_{yx} and h_{yy} are expressed as the following:

$$h_{xx} = \sum_{j=1}^{N} g(\phi j(t))\sin(\phi j(t))[Ktc\cos(\phi j(t)) + Knc\sin(\phi j(t))] \tag{8}$$

$$h_{xy} = \sum_{j=1}^{N} g(\phi j(t))\cos(\phi j(t))[Ktc\cos(\phi j(t)) + Knc\sin(\phi j(t))] \tag{9}$$

$$h_{yx} = \sum_{j=1}^{N} g(\phi j(t))\sin(\phi j(t))[-Ktc\sin(\phi j(t)) + Knc\cos(\phi j(t))] \tag{10}$$

$$h_{yy} = \sum_{j=1}^{N} g(\phi j(t))\cos(\phi j(t))[-Ktc\sin(\phi j(t)) + Knc\cos(\phi j(t))] \tag{11}$$

Let $\mathbf{U} = [x(t)\ \ y(t)\ \ \dot{x}(t)\ \ \dot{y}(t)]^T$, then Eq. (7) can be rewritten in the following state space form:

$$\dot{\mathbf{U}}(t) = \mathbf{A}\cdot\mathbf{U}(t) + \mathbf{L}(t)[\mathbf{U}(t)-\mathbf{U}(t-\tau)] \tag{12}$$

$$\mathbf{A} = \begin{bmatrix} 0 & 0 & 1 & 0 \\ 0 & 0 & 0 & 1 \\ p1 & p2 & e1 & e2 \\ p3 & p4 & e3 & e4 \end{bmatrix}; \mathbf{L}(t) = \begin{bmatrix} 0 & 0 & 0 & 0 \\ 0 & 0 & 0 & 0 \\ o1 & o2 & 0 & 0 \\ o3 & o4 & 0 & 0 \end{bmatrix} \tag{13}$$

Equation 12 is the state space form of the mathematical model of milling process which takes regenerative effect and mode coupling effect into account.

Where

$$p1 = -\frac{m_y k_x}{m_x m_y - m_{xy} m_{yx}} + \frac{m_{xy} m_{yx}}{m_x m_y - m_{xy} m_{yx}} \tag{14}$$

$$p2 = -\frac{m_y k_{xy}}{m_x m_y - m_{xy} m_{yx}} + \frac{m_{xy} k_y}{m_x m_y - m_{xy} m_{yx}} \tag{15}$$

$$p3 = \frac{m_{yx} k_x}{m_x m_y - m_{xy} m_{yx}} - \frac{m_x k_{yx}}{m_x m_y - m_{xy} m_{yx}} \tag{16}$$

$$p4 = \frac{m_{yx} k_{xy}}{m_x m_y - m_{xy} m_{yx}} - \frac{m_x k_y}{m_x m_y - m_{xy} m_{yx}} \tag{17}$$

$$e1 = -\frac{m_y c_x}{m_x m_y - m_{xy} m_{yx}} + \frac{m_{xy} c_{yx}}{m_x m_y - m_{xy} m_{yx}} \tag{18}$$

$$e2 = -\frac{m_y c_{xy}}{m_x m_y - m_{xy} m_{yx}} + \frac{m_{xy} c_y}{m_x m_y - m_{xy} m_{yx}} \tag{19}$$

$$e3 = \frac{m_{yx} c_x}{m_x m_y - m_{xy} m_{yx}} - \frac{m_x c_{yx}}{m_x m_y - m_{xy} m_{yx}} \tag{20}$$

$$e4 = \frac{m_{yx} c_{xy}}{m_x m_y - m_{xy} m_{yx}} - \frac{m_x c_y}{m_x m_y - m_{xy} m_{yx}} \tag{21}$$

$$o1 = -\frac{m_y \cdot a_p \cdot h_{xx}}{m_x m_y - m_{xy} m_{yx}} + \frac{m_{xy} \cdot a_p \cdot h_{yx}}{m_x m_y - m_{xy} m_{yx}} \tag{22}$$

$$o2 = -\frac{m_y \cdot a_p \cdot h_{xy}}{m_x m_y - m_{xy} m_{yx}} + \frac{m_{xy} \cdot a_p \cdot h_{yy}}{m_x m_y - m_{xy} m_{yx}} \tag{23}$$

$$o3 = \frac{m_{yx} \cdot a_p \cdot h_{xx}}{m_x m_y - m_{xy} m_{yx}} - \frac{m_x \cdot a_p \cdot h_{yx}}{m_x m_y - m_{xy} m_{yx}} \tag{24}$$

$$o4 = \frac{m_{yx} \cdot a_p \cdot h_{xy}}{m_x m_y - m_{xy} m_{yx}} - \frac{m_x \cdot a_p \cdot h_{yy}}{m_x m_y - m_{xy} m_{yx}} \tag{25}$$

2.2 Dynamical model of milling process by considering regenerative effect, mode coupling effect, and process damping

The process damping is caused by the indentation of undulations under the flank face of the tool at the interface between the tool and workpiece. As shown in Fig. 2, S denotes the area of the cross section of the extruded material; w is the wear land width of the tool.

According to Ahmadi et al. [32], the radial plowing force can be assumed to be proportional to the volume of the material extruded underneath the flank face.

$$Fpd,r = g(\phi j)\cdot Ksp\cdot ap\cdot S \tag{26}$$

where K_{sp} is the specific indentation force, the details of it can be found in Refs [38–40]. S denotes the area of the cross section of the extruded material, as shown in Fig. 2.

The tangential plowing force can be described by the Coulomb friction, as shown in the following equation

$$Fpd,t = \mu\cdot Fpd,r \tag{27}$$

where μ is the Coulomb friction coefficient which is related to the workpiece material and the cutting conditions.

Ahmadi et al. [32] pointed out that the process damping effect can be represented by an equivalent linear viscous damper.

$$Fpd,r \approx C_{eq}\cdot\dot{r}(t); C_{eq} = K_{sp}a_p\frac{w^2}{4v} \tag{28}$$

where $\dot{r}(t) = \dot{x}(t)\sin\phi j(t) + \dot{y}(t)\cos\phi j(t)$, w is the wear land width of the tool as shown in Fig. 2. v is the tangential velocity $v = \pi D\Omega/60$, D denotes the tool diameter.

The process damping force can be expressed in the X and Y directions as the following equation

$$\mathbf{F}p = \begin{bmatrix} Fpx \\ Fpy \end{bmatrix} = \sum_{j=1}^{N} \begin{bmatrix} -\cos\phi j & -\sin\phi j \\ \sin\phi j & -\cos\phi j \end{bmatrix} \begin{bmatrix} Fpd,t \\ Fpd,r \end{bmatrix} \tag{29}$$

$$\begin{bmatrix} Fpd,t \\ Fpd,r \end{bmatrix} = g(\phi j)Ceq \begin{bmatrix} \mu \\ 1 \end{bmatrix} [\sin(\phi j) \quad \cos(\phi j)] \begin{bmatrix} \dot{x}(t) \\ \dot{y}(t) \end{bmatrix} \tag{30}$$

Equation (29) can be rewritten as

$$\mathbf{F}p = \begin{bmatrix} Fpx \\ Fpy \end{bmatrix} = -Ceq \begin{bmatrix} c_{p,x} & c_{p,xy} \\ c_{p,yx} & c_{p,y} \end{bmatrix} \begin{bmatrix} \dot{x}(t) \\ \dot{y}(t) \end{bmatrix} \tag{31}$$

where

$$c_{p,x} = \sum_{j=1}^{N} g(\phi j)\sin(\phi j)[\sin(\phi j) + \mu\cos(\phi j)] \tag{32}$$

$$c_{p,xy} = \sum_{j=1}^{N} g(\phi j)\cos(\phi j)[\sin(\phi j) + \mu\cos(\phi j)] \tag{33}$$

$$c_{p,yx} = \sum_{j=1}^{N} g(\phi j)\sin(\phi j)[\cos(\phi j) - \mu\sin(\phi j)] \tag{34}$$

$$c_{p,y} = \sum_{j=1}^{N} g(\phi j)\cos(\phi j)[\cos(\phi j) - \mu\sin(\phi j)] \tag{35}$$

The dynamical equation of milling process considering regenerative effect, mode coupling effect, and process damping can be expressed as follows

$$\begin{bmatrix} m_x & m_{xy} \\ m_{yx} & m_y \end{bmatrix} \begin{bmatrix} \ddot{x}(t) \\ \ddot{y}(t) \end{bmatrix} + \begin{bmatrix} c_x & c_{xy} \\ c_{yx} & c_y \end{bmatrix} \begin{bmatrix} \dot{x}(t) \\ \dot{y}(t) \end{bmatrix} + \begin{bmatrix} k_x & k_{xy} \\ k_{yx} & k_y \end{bmatrix} \begin{bmatrix} x(t) \\ y(t) \end{bmatrix} = \begin{bmatrix} Fx(t) \\ Fy(t) \end{bmatrix} + \begin{bmatrix} Fpx(t) \\ Fpy(t) \end{bmatrix} \tag{36}$$

Substituting Eq. (2), (3), (31) into Eq. (36), the following equation can be obtained.

$$\begin{bmatrix} m_x & m_{xy} \\ m_{yx} & m_y \end{bmatrix} \begin{bmatrix} \ddot{x}(t) \\ \ddot{y}(t) \end{bmatrix} + \begin{bmatrix} c_x & c_{xy} \\ c_{yx} & c_y \end{bmatrix} \begin{bmatrix} \dot{x}(t) \\ \dot{y}(t) \end{bmatrix} + Ceq \begin{bmatrix} c_{p,x} & c_{p,xy} \\ c_{p,yx} & c_{p,y} \end{bmatrix} \begin{bmatrix} \dot{x}(t) \\ \dot{y}(t) \end{bmatrix} + \begin{bmatrix} k_x & k_{xy} \\ k_{yx} & k_y \end{bmatrix} \begin{bmatrix} x(t) \\ y(t) \end{bmatrix} = \begin{bmatrix} -a_p h_{xx} & -a_p h_{xy} \\ -a_p h_{yx} & -a_p h_{yy} \end{bmatrix} \begin{bmatrix} x(t) \\ y(t) \end{bmatrix} - \begin{bmatrix} -a_p h_{xx} & -a_p h_{xy} \\ -a_p h_{yx} & -a_p h_{yy} \end{bmatrix} \begin{bmatrix} x(t-T) \\ y(t-T) \end{bmatrix} + \mathbf{F}_0 \tag{37}$$

As discussed in Sect. 2.1, the steady force excitation $\mathbf{F}_0$ can be ignored, let $\mathbf{U} = [x(t) \;\; y(t) \;\; \dot{x}(t) \;\; \dot{y}(t)]^T$, and then Eq. (37) can be rewritten in the following state space form:

$$\dot{\mathrm{U}}(t) = \mathbf{A}\mathbf{U}(t) + \mathbf{R}(t)\mathbf{U}(t) - \mathbf{L}(t)\mathbf{U}(t-\tau) \tag{38}$$

where

$$\mathbf{A} = \begin{bmatrix} 0 & 0 & 1 & 0 \\ 0 & 0 & 0 & 1 \\ p1 & p2 & e1 & e2 \\ p3 & p4 & e3 & e4 \end{bmatrix} \tag{39}$$

$$\mathbf{R}(t) = \begin{bmatrix} 0 & 0 & 0 & 0 \\ 0 & 0 & 0 & 0 \\ o1 & o2 & f1{\cdot}Ceq & f2{\cdot}Ceq \\ o3 & o4 & f3{\cdot}Ceq & f4{\cdot}Ceq \end{bmatrix}, \mathrm{L}(t) = \begin{bmatrix} 0 & 0 & 0 & 0 \\ 0 & 0 & 0 & 0 \\ o1 & o2 & 0 & 0 \\ o3 & o4 & 0 & 0 \end{bmatrix} \tag{40}$$

where

$$f1 = -\frac{m_y{\cdot}c_{p,x}}{m_x m_y - m_{xy}m_{yx}} + \frac{m_{xy}{\cdot}c_{p,yx}}{m_x m_y - m_{xy}m_{yx}} \tag{41}$$

$$f2 = -\frac{m_y{\cdot}c_{p,xy}}{m_x m_y - m_{xy}m_{yx}} + \frac{m_{xy}{\cdot}c_{p,y}}{m_x m_y - m_{xy}m_{yx}} \tag{42}$$

$$f3 = \frac{m_{yx}{\cdot}c_{p,x}}{m_x m_y - m_{xy}m_{yx}} - \frac{m_x{\cdot}c_{p,yx}}{m_x m_y - m_{xy}m_{yx}} \tag{43}$$

$$f4 = \frac{m_{yx}{\cdot}c_{p,xy}}{m_x m_y - m_{xy}m_{yx}} - \frac{m_x{\cdot}c_{p,y}}{m_x m_y - m_{xy}m_{yx}} \tag{44}$$

3 Milling chatter stability prediction

Usually, the stability prediction is based on the stability lobe diagrams (SLD). When the parameter combination (i.e., the spindle speed and the axial depth of cut) is beyond the stability boundaries, the milling system is unstable; when the parameter combination is below the stability boundaries, the milling system is considered stable. In this paper, the full discretization method (FDM) is utilized to obtain the SLD.

3.1 FDM method for chatter stability prediction

In this paper, we use an updated full discretization method (FDM) [41] which is based on the third-order Hermite-Newton interpolation polynomial to obtain the SLD. In this method, by dividing the tooth passing period equally into a finite set of time intervals, the third-order Hermite interpolation polynomial and the third-order Newton interpolation polynomial are utilized in each time interval to estimate the state item and the time-delayed item, respectively. And the time-periodic matrices are approximated by the first-order Lagrange interpolation polynomial. This method shows a faster convergence rate than that of other methods, and its SLD is more close to the ideal ones with small number of time intervals. The brief introduction of the updated FDM is described as follows.

Based on the third-order (four nodes) Newton interpolation polynomial, the time-delayed item U($s-\tau$)of the state-space

equation in the time span $[t_i, t_{i+1}]$ could be approximated by Eq. (45).

$$\mathbf{U}(s\text{-}\tau)\approx\mathbf{a}_1\mathrm{U}_{i-n}+\mathbf{b}_1\mathbf{U}_{i-n+1}+\mathbf{c}_1\mathbf{U}_{i-n+2}+\mathbf{d}_1\mathbf{U}_{i-n+3} \tag{45}$$

where

$$\mathbf{a}_1=\left(1-\frac{11s}{6h}+\frac{s^2}{h^2}-\frac{s^3}{6h^3}\right)\mathbf{I} \tag{46}$$

$$\mathbf{b}_1=\left(\frac{3s}{h}-\frac{5s^2}{2h^2}+\frac{s^3}{2h^3}\right)\mathbf{I} \tag{47}$$

$$\mathbf{c}_1=\left(-\frac{3s}{2h}+\frac{2s^2}{h^2}-\frac{s^3}{2h^3}\right)\mathbf{I} \tag{48}$$

$$\mathbf{d}_1=\left(\frac{s}{3h}-\frac{s^2}{2h^2}+\frac{s^3}{6h^3}\right)\mathbf{I} \tag{49}$$

The state item is approximated by the third-order Hermite interpolation polynomial method, as shown in Eq. (50).

$$\mathbf{U}(s)\approx\mathbf{a}_2\mathbf{U}_i+\mathbf{b}_2\mathbf{U}_{i+1}+\mathbf{c}_2\mathbf{U}_{i-n}+\mathbf{d}_2\mathbf{U}_{i-n+1} \tag{50}$$

where

$$\mathbf{a}_2=\frac{(s-h)^2((\mathbf{I}+(\mathbf{A}+\mathbf{R}_i)s)h+2s\mathbf{I})}{h^3} \tag{51}$$

$$\mathbf{b}_2=\frac{((3\mathbf{I}+(\mathbf{A}+\mathbf{R}_{i+1})s)h-(\mathbf{A}+\mathbf{R}_{i+1})h^2-2s\mathbf{I})s^2}{h^3} \tag{52}$$

$$\mathbf{c}_2=-\frac{(s-h)^2s}{h^2}\mathbf{L}_i,\ \mathbf{d}_2=-\frac{s^2(s-h)}{h^2}\mathbf{L}_{i+1} \tag{53}$$

The comparison of local discretization error between different methods for a three-axis milling system is conducted. The single degree of freedom (single-DOF) fully-immersed milling system [12] (just considering the feed direction) is utilized to analyze the convergence rate of the third-order Hermite-Newton (3rdH-NAM) and other FDM methods. The exact eigenvalue μ_0 is determined by the 1stSDM with $m=200$. To compare the convergence rate of different computing methods, the system parameters are the same as literature [11], i.e., the natural frequency ω_n=2π × 922 Hz, the relative damping ζ = 0.011, the modal mass m=0.03993 kg, the radial immersion ratio a_e/D=1, the tangential and the normal linearized cutting force coefficient K_t=6 × 10^8 N/m^2 and K_n=2 × 10^8 N/m^2, the number of the cutter teeth $N=2$, the spindle speed Ω = 5000 rpm, Ω = 5000 rpm, Ω = 6800 rpm, and Ω = 12,000 rpm, respectively. The axial depth of cut a_p is set as 0.2, 0.5, 2.7, and 1.5 mm, respectively, down-milling. The comparison of the convergence rate of the first-order semi-discretization method (1stSDM) [42], the third-order full-discretization method (3rdFDM) [43], the third-order Hermite approximation methods (3rdHAM [44]), and the third-order Hermite-Newton (3rdH-NAM) are shown in Fig. 3.

It is clear from Fig. 3 that the third-order Hermite approximation method (3rdH-NAM) shows a faster convergence rate than that of other methods.

The detailed introduction of the 3rdH-NAM can be found in Ref [41].

3.2 Chatter stability prediction by considering the multiple factors coupling effects

When the updated full discretization method (FDM) [41] is utilized to obtain the SLD, the time-periodic matrices $\mathbf{R}(t)$ and $\mathbf{L}(t)$ of eq. (38) are approximated by the first-order Lagrange interpolation polynomial, respectively. That is

$$\mathbf{R}(s)\approx\frac{h-s}{h}\mathbf{R}_i+\frac{s}{h}\mathbf{R}_{i+1} \tag{54}$$

$$\mathbf{L}(s)\approx\frac{h-s}{h}\mathbf{L}_i+\frac{s}{h}\mathbf{L}_{i+1} \tag{55}$$

In Eq. (38), the time delay τ is equal to the tooth pass period T, i.e., τ = T. To solve Eq. (38), the time period is divided into n time intervals, then each interval length $h=\tau/n$. The time intervals can be expressed by $[t_i, t_{i+1}]$, $i=1, 2,\ldots, n$. Equation (38) is integrated on the ith small time interval$[t_i \le s \le t_{i+1}]$; the result is shown as Eq. (56).

$$\mathbf{U}_{i+1}=e^{\mathbf{A}h}\mathbf{U}_i+\int_{t_i}^{t_{i+1}}e^{\mathbf{A}(t_{i+1}-s)}[\mathbf{R}(s)\mathbf{U}(s)-\mathbf{L}(s)\mathbf{U}(s-\tau)]ds \tag{56}$$

Substituting Eqs. (45), (50), (54), and (55) into Eq. (56) yields

$$\mathbf{U}_{i+1}=\mathbf{P}_i\begin{bmatrix}(e^{\mathbf{A}h}+\mathbf{G}_{13}\mathbf{R}_{i+1}+\mathbf{G}_{14}\mathbf{R}_i)\mathbf{U}_i\\-(\mathbf{G}_{15}\mathbf{L}_{i+1}+\mathbf{G}_{16}\mathbf{L}_i)\mathbf{U}_{i-n+3}\\-(\mathbf{G}_{17}\mathbf{L}_{i+1}+\mathbf{G}_{18}\mathbf{L}_i)\mathbf{U}_{i-n+2}\\+[(\mathbf{G}_{19}\mathbf{R}_{i+1}+\mathbf{G}_{20}\mathbf{R}_i)-(\mathbf{G}_{21}\mathbf{L}_{i+1}+\mathbf{G}_{22}\mathbf{L}_i)]\mathbf{U}_{i-n+1}\\+[(\mathbf{G}_{23}\mathbf{R}_{i+1}+\mathbf{G}_{24}\mathbf{R}_i)-(\mathbf{G}_{25}\mathbf{L}_{i+1}+\mathbf{G}_{26}\mathbf{L}_i)]\mathbf{U}_{i-n}\end{bmatrix} \tag{57}$$

where

$$\mathbf{P}_i=[\mathbf{I}-\mathbf{G}_{11}\mathbf{R}_i-\mathbf{G}_{12}\mathbf{R}_{i+1}]^{-1} \tag{58}$$

$$\mathbf{G}_{11}=\left(-\frac{\mathbf{R}_{i+1}}{h^3}+\frac{2\mathbf{I}}{h^4}-\frac{\mathbf{A}}{h^3}\right)\mathbf{F}_4+\left(\frac{2\mathbf{A}}{h^2}+\frac{2\mathbf{R}_{i+1}}{h^2}-\frac{5\mathbf{I}}{h^3}\right)\mathbf{F}_3+\left(\frac{3\mathbf{I}}{h^2}-\frac{\mathbf{A}}{h}-\frac{\mathbf{R}_{i+1}}{h}\right)\mathbf{F}_2 \tag{59}$$

$$\mathbf{G}_{12}=\left(\frac{\mathbf{A}}{h^3}+\frac{\mathbf{R}_{i+1}}{h^3}-\frac{2\mathbf{I}}{h^4}\right)\mathbf{F}_4+\left(\frac{3\mathbf{I}}{h^3}-\frac{\mathbf{A}}{h^2}-\frac{\mathbf{R}_{i+1}}{h^2}\right)\mathbf{F}_3 \tag{60}$$

$$\mathbf{G}_{13}=\frac{\mathbf{F}_1}{h}+\left(\frac{\mathbf{A}}{h}+\frac{\mathbf{R}_i}{h}\right)\mathbf{F}_2-\left(\frac{2\mathbf{R}_i}{h^2}+\frac{2\mathbf{A}}{h^2}+\frac{3\mathbf{I}}{h^3}\right)\mathbf{F}_3+\left(\frac{2\mathbf{I}}{h^4}+\frac{\mathbf{A}}{h^3}+\frac{\mathbf{R}_i}{h^3}\right)\mathbf{F}_4 \tag{61}$$

$$\mathbf{G}_{14}=\left(\frac{5\mathbf{I}}{h^3}+\frac{3\mathbf{A}}{h^2}+\frac{3\mathbf{R}_i}{h^2}\right)\mathbf{F}_3+\mathbf{F}_0+\left(\mathbf{R}_i+\mathbf{A}-\frac{\mathbf{I}}{h}\right)\mathbf{F}_1-\left(\frac{3\mathbf{A}}{h}+\frac{3\mathbf{I}}{h^2}+\frac{3\mathbf{R}_i}{h}\right)\mathbf{F}_2-\left(\frac{2\mathbf{I}}{h^4}+\frac{\mathbf{A}}{h^3}+\frac{\mathbf{R}_i}{h^3}\right)\mathbf{F}_4 \tag{62}$$

$$\mathbf{G}_{15}=\frac{\mathbf{F}_4}{6h^4}-\frac{\mathbf{F}_3}{2h^3}+\frac{\mathbf{F}_2}{3h^2} \tag{63}$$

$$\mathbf{G}_{16}=\frac{-\mathbf{F}_4}{6h^4}+\frac{2\mathbf{F}_3}{3h^3}-\frac{5\mathbf{F}_2}{6h^2}+\frac{\mathbf{F}_1}{3h} \tag{64}$$

$$\mathbf{G}_{17}=\frac{-\mathbf{F}_4}{2h^4}+\frac{2\mathbf{F}_3}{h^3}-\frac{3\mathbf{F}_2}{2h^2} \tag{65}$$

$$\mathbf{G}_{18}=\frac{\mathbf{F}_4}{2h^4}-\frac{5\mathbf{F}_3}{2h^3}+\frac{7\mathbf{F}_2}{2h^2}-\frac{3\mathbf{F}_1}{2h} \tag{66}$$

$$\mathbf{G}_{19}=-\frac{\mathbf{L}_{i+1}}{h^3}\mathbf{F}_4+\frac{\mathbf{L}_{i+1}}{h^2}\mathbf{F}_3 \tag{67}$$

$$\mathbf{G}_{20}=\left(\frac{\mathbf{F}_2}{h}-\frac{2\mathbf{F}_3}{h^2}+\frac{\mathbf{F}_4}{h^3}\right)\mathbf{L}_{i+1} \tag{68}$$

$$\mathbf{G}_{21}=\frac{3\mathbf{F}_2}{h^2}-\frac{5\mathbf{F}_3}{2h^3}+\frac{\mathbf{F}_4}{2h^4} \tag{69}$$

$$\mathbf{G}_{22}=\frac{3\mathbf{F}_1}{h}-\frac{11\mathbf{F}_2}{2h^2}+\frac{3\mathbf{F}_3}{h^3}-\frac{\mathbf{F}_4}{2h^4} \tag{70}$$

$$\mathbf{G}_{23}=\left(-\frac{\mathbf{F}_2}{h}+\frac{2\mathbf{F}_3}{h^2}-\frac{\mathbf{F}_4}{h^3}\right)\mathbf{L}_i \tag{71}$$

$$\mathbf{G}_{24}=\left(-\mathbf{F}_1+\frac{3\mathbf{F}_2}{h}-\frac{3\mathbf{F}_3}{h^2}+\frac{\mathbf{F}_4}{h^3}\right)\mathbf{L}_i \tag{72}$$

$$\mathbf{G}_{25}=\frac{\mathbf{F}_1}{h}-\frac{11\mathbf{F}_2}{6h^2}+\frac{\mathbf{F}_3}{h^3}-\frac{\mathbf{F}_4}{6h^4} \tag{73}$$

$$\mathbf{G}_{26}=\mathbf{F}_0-\frac{17\mathbf{F}_1}{6h}+\frac{17\mathbf{F}_2}{6h^2}-\frac{7\mathbf{F}_3}{6h^3}+\frac{\mathbf{F}_4}{6h^4} \tag{74}$$

$$\mathbf{F}_0=\mathbf{A}^{-1}\left(e^{\mathbf{A}h}-\mathbf{I}\right),\ \mathbf{F}_1=\mathbf{A}^{-1}\left(\mathbf{F}_0-h\mathbf{I}\right) \tag{75}$$

$$\mathbf{F}_2=\mathbf{A}^{-1}\left(2\mathbf{F}_1-h^2\mathbf{I}\right),\ \mathbf{F}_3=\mathbf{A}^{-1}\left(3\mathbf{F}_2-h^3\mathbf{I}\right) \tag{76}$$

$$\mathbf{F}_4=\mathbf{A}^{-1}\left(4\mathbf{F}_3-h^4\mathbf{I}\right),\quad \mathbf{F}_5=\mathbf{A}^{-1}\left(5\mathbf{F}_4-h^5\mathbf{I}\right) \tag{77}$$

If P_i is a nonsingular matrix, the local discrete mapping can be expressed as matrix form according to Eq. (57), as shown in Eq. (78).

$$\begin{Bmatrix}\mathbf{U}_{i+1}\\ \mathbf{U}_i\\ \mathbf{U}_{i-1}\\ \vdots\\ \mathbf{U}_{i+1-n}\end{Bmatrix}=\mathbf{N}_i\begin{Bmatrix}\mathbf{U}_i\\ \mathbf{U}_{i-1}\\ \mathbf{U}_{i-2}\\ \vdots\\ \mathbf{U}_{i-n}\end{Bmatrix} \tag{78}$$

where N_i can be expressed in Eq. (79):

$$\mathbf{N}_i=\begin{bmatrix}\mathbf{N}^i_{11} & 0 & \cdots & \mathbf{N}^i_{1,n-2} & \mathbf{N}^i_{1,n-1} & \mathbf{N}^i_{1,n} & \mathbf{N}^i_{1,n+1}\\ \mathbf{I} & 0 & \cdots & 0 & 0 & 0 & 0\\ 0 & \mathbf{I} & \cdots & 0 & 0 & 0 & 0\\ \vdots & \vdots & \vdots & \vdots & \vdots & \vdots & \vdots\\ 0 & 0 & \cdots & 0 & 0 & \mathbf{I} & 0\end{bmatrix} \tag{79}$$

In Eq. (79), the matrices $\mathbf{N}^i_{11}$,$\mathbf{N}^i_{1,n-2}$,$\mathbf{N}^i_{1,n-1}$,$\mathbf{N}^i_{1,n}$, $\mathbf{N}^i_{1,n+1}$ are expressed as Eqs. (80)–(84), respectively.

$$\mathbf{N}^i_{11}=\mathbf{P}_i\left(e^{\mathbf{A}h}+\mathbf{G}_{13}\mathbf{R}_{i+1}+\mathbf{G}_{14}\mathbf{R}_i\right) \tag{80}$$

$$\mathbf{N}^i_{1,n-2}=-\mathbf{P}_i(\mathbf{G}_{15}\mathbf{L}_{i+1}+\mathbf{G}_{16}\mathbf{L}_i) \tag{81}$$

$$\mathbf{N}^i_{1,n-1}=-\mathbf{P}_i(\mathbf{G}_{17}\mathbf{L}_{i+1}+\mathbf{G}_{18}\mathbf{L}_i) \tag{82}$$

$$\mathbf{N}^i_{1,n}=\mathbf{P}_i[(\mathbf{G}_{19}\mathbf{R}_{i+1}+\mathbf{G}_{20}\mathbf{R}_i)-(\mathbf{G}_{21}\mathbf{L}_{i+1}+\mathbf{G}_{22}\mathbf{L}_i)] \tag{83}$$

$$\mathbf{N}^i_{1,n+1}=\mathbf{P}_i[(\mathbf{G}_{23}\mathbf{R}_{i+1}+\mathbf{G}_{24}\mathbf{R}_i)-(\mathbf{G}_{25}\mathbf{L}_{i+1}+\mathbf{G}_{26}\mathbf{L}_i)] \tag{84}$$

The state transition matrix ψ for the dynamic system over one period T can be written as

$$\boldsymbol{\psi}=\mathbf{N}_n\mathbf{N}_{n-1}\cdots\mathbf{N}_1 \tag{85}$$

Then, the stability of the system can be determined according to the Floquet theory [45].

4 The verification

To verify the proposed milling dynamical model, both numerical simulation analysis and milling experiments are conducted. The results show that both of the regenerative effect, mode coupling effect, and process damping have significant influence on the SLD, and the proposed dynamical model is more consistent with the actual milling situation.

4.1 Numerical simulation

To investigate the influences of mode coupling effect and process damping on the SLD, a series of numerical simulations are conducted. The operations are 1/2 immersion up-milling and down-milling, respectively; the workpiece is aluminum block. The parameters from Ref. [46] are used for the simulation case, as shown in Table 1.

In this section, the stability lobe diagrams (SLD) are calculated by the updated full discretization method [41] with time intervals $m = 50$ over a 200×200 sized grid of spindle speed Ω and the axial depth of cut a_p. In the SLD, the axial depth of cut ranges from 0 to 0.01 m; the spindle speed ranges from 1×10^3 to 10×10^3 rpm.

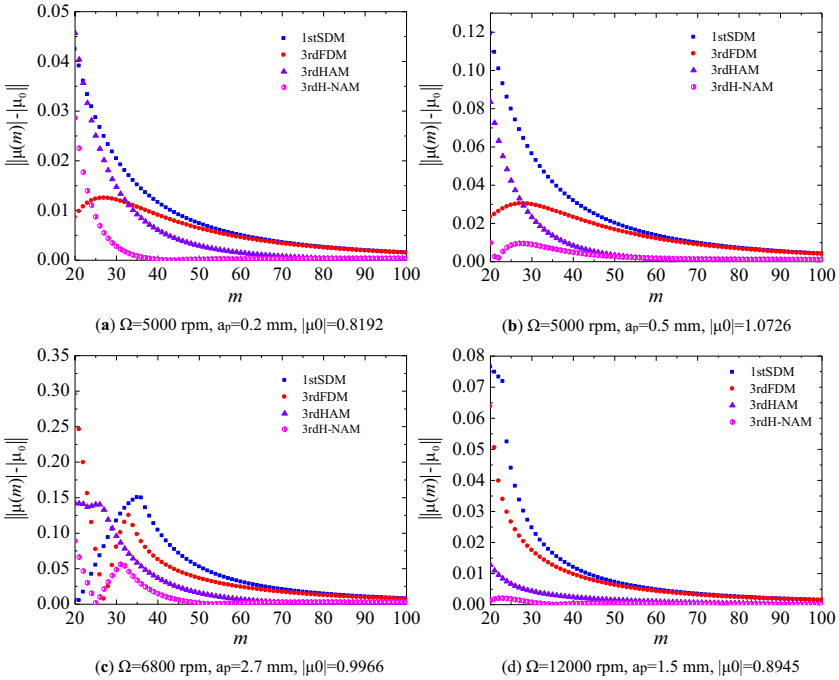

Fig. 3 Convergence rate of eigenvalues for different approximation parameters n for the 1stSDM, the 3rdFDM, the 3rdHAM, and the 3rdH-NAM methods

The SLDs which are obtained by considering the process damping and without the process damping are shown in Fig. 4. It is clear from Fig. 4 that at the low speed region, there are no whole lobes for reference if the process damping is ignored (the red line). However, there exist relative large stability areas at the low speed region when the process damping is considered (the blue line).

For down-milling operation, the SLDs which are obtained by considering the process damping (1/2 immersion) and without it are shown in Fig. 5. Compared to Fig. 4, it is clear from Fig. 5 that although the shape of the SLDs for down-milling is different with the SLDs for up-milling, the influence of process damping on the SLD is still mainly reflected in low-speed cutting region.

Gradisek et al. [48] pointed out that even the cross terms in magnitude only 2% that of the direct terms, it may also influence the predicted stability boundary, and Refs [22, 49] show that cross terms in magnitude are more than 80% that of the direct terms according to the experiment test. Inspired by this conclusion, when comparing the influence of mode on the stability boundaries, for clarity, we assume that the cross terms are determined as 60% of the values of each direct term (in this section, we just want to verify the influence of mode coupling effect on SLDs, more precise parameter testing will be

Table 1 The parameters for simulation [46]

Items	Value
Tool diameter	25.4 mm
The wear land w	0.08 mm
Tooth number N	3
a_e/D	0.5
K_x	5.6×10^6 N/m
K_y	5.7×10^6 N/m
C_x	115.29 Ns/m
C_y	95.35 Ns/m
M_x	0.39 kg
M_y	0.32 kg
f_x	603 Hz
f_y	666 Hz
K_t	700 MPa
K_r	0.07
K_{sp} [47]	1.5×10^{14} N/m^3
μ	0.3

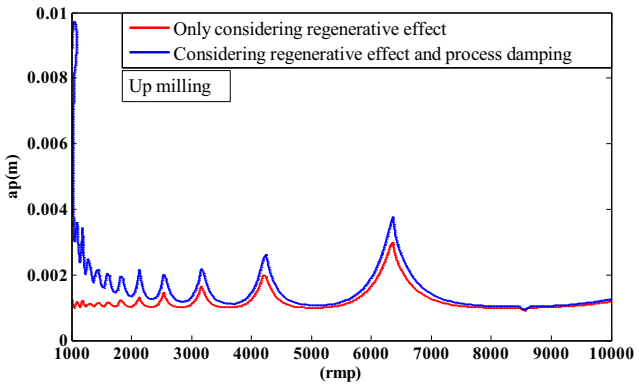

Fig. 4 The SLDs for up-milling (1/2 immersion) by considering the process damping (the blue line) and without it (the red line)

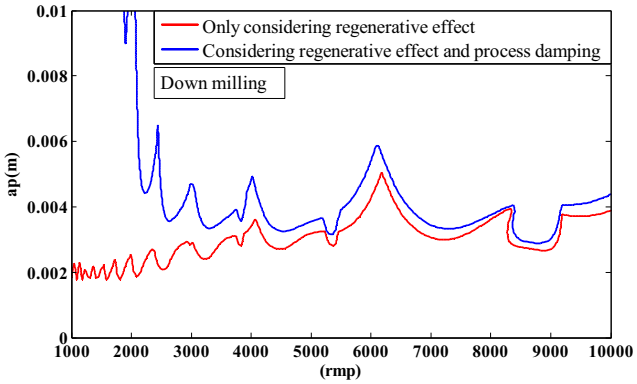

Fig. 5 The SLDs for down-milling (1/2 immersion) by considering the process damping (the blue line) and without it (the red line)

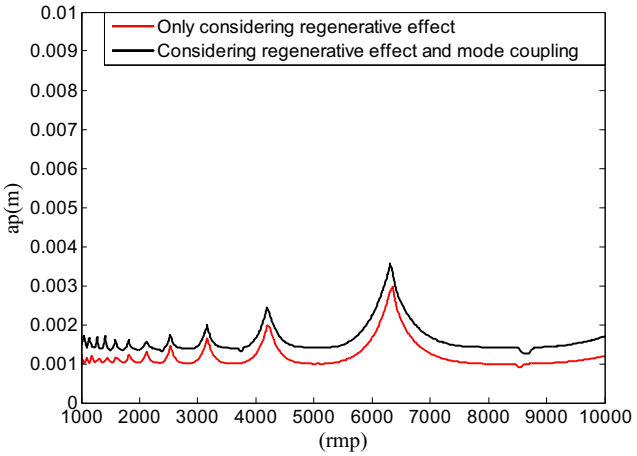

Fig. 6 The SLD for up-milling (1/2 immersion) by considering the mode coupling (the black line) and without it (the red line)

conducted in the experimental validation section). So, the parameters can be determined as

$$Kxy = Kx \times 60\% = 3.36 \times 10^6 N/m \tag{86}$$

$$Kyx = Ky \times 60\% = 3.42 \times 10^6 N/m \tag{87}$$

$$Cxy = Cx \times 60\% = 69.174 Ns/m \tag{88}$$

$$Cyx = Cy \times 60\% = 57.21 Ns/m \tag{89}$$

$$Mxy = Mx \times 60\% = 0.234 Kg \tag{90}$$

$$Myx = My \times 60\% = 0.192 Kg \tag{91}$$

It is clear from Fig. 6 that the SLD which considers mode coupling effect changes a lot compared with the SLD without mode coupling effect. Since the value of the cross terms is obtained by assumption, the result may be not accurate, but according to it, we can get the conclusion that the mode coupling effects have influence on the stability boundaries. In Sect. 4.2, the exact value of the cross terms will be tested by experiment.

When simultaneously considering the multiple factor coupling effects, i.e., regenerative effect, mode coupling effect, and process damping, the SLD is shown in Fig. 7. As shown in Fig. 7, the red line represents the SLD obtained by only considering the regenerative effect; the blue line represents the SLD obtained by considering the regenerative effect and process damping; the green line represents the SLD obtained by considering the regenerative effect and mode coupling effect; the black line represents the SLD obtained by simultaneously considering the regenerative effect, mode coupling, and process damping.

It is clear from Fig. 7 that both of the regenerative effect, mode coupling effect, and process damping have significant influence on the SLD. In the low speed region, when taking the regenerative effect, process damping, and mode coupling effect into account, the stability region is relatively large.

As discussed by Balachandran and Zhao [20], Balachandran and Long [50], the SLDs for up-milling and down-milling operations are different.

To study the influence of the multiple factor coupling effects (simultaneously considering the regenerative effect, mode coupling, and process damping) on the stability regions of down-milling operation, the numerical simulation for the down-milling operation with the same simulation parameters as Fig. 7 is carried out.

Figure 8 shows the SLDs for down-milling operation. For simplicity, and to emphasize the critical factors, Fig. 8 only displays the SLDs obtained by the traditional dynamical model (only considering the regenerative effect) and the proposed dynamical model (simultaneously considering the regenerative effect, mode coupling, and process damping). The SLDs of Fig. 8 also indicate that the stability region is relatively large when taking the regenerative effect, process damping, and mode coupling effect into account.

For purpose of studying the influence of radial immersion ratio (a_e/D) and the multiple factor coupling effects on the SLDs of up-milling and down-milling operations, and comparing the SLDs' differences between these two milling operations (up-milling and down-milling), a series of numerical simulations are carried out. The parameters for simulations are shown in Table 1 and Eqs (86)–(91). The simulation results for up-milling and down-milling operations with different radial immersion ratios are shown in Fig. 9.

It is clear from Fig. 9 that the SLDs generated for up-milling and down-milling operations are also different when taking the multiple factors (simultaneously considering the regenerative effect, mode coupling, and process damping) coupling effects into account. When the SLDs are presented for low radial immersion operations, the stability region for

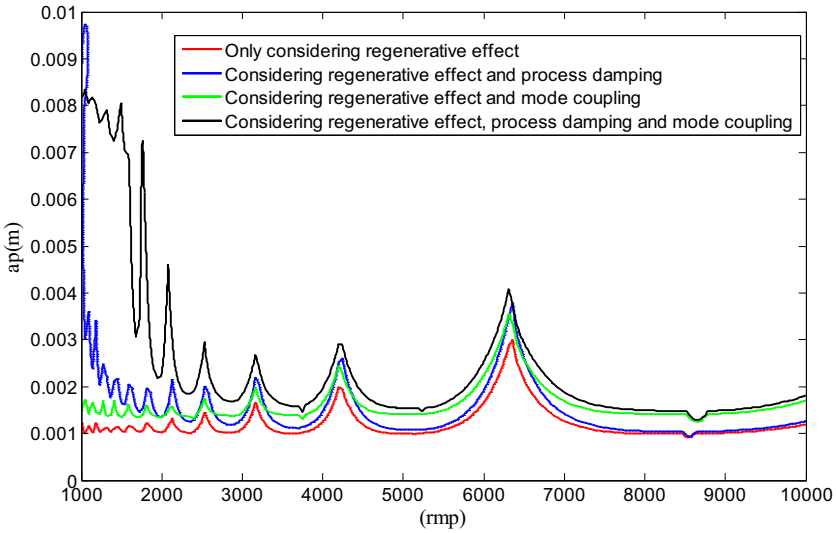

Fig. 7 The SLD for up-milling (1/2 immersion) by considering the regenerative effect (the red line); the regenerative effect and process damping (the blue line); the regenerative effect and mode coupling (the green line); the regenerative effect, mode coupling, and process damping (the black line)

up-milling operations is larger than that for down-milling operations, as shown in Fig. 9a–c, while with the increase of the radial immersion ratio (a_e/D), the stability region for up-milling operations is less than that for down-milling operations, as shown in Fig. 9e–i; then, the SLDs for the two operations are in proximity to each other (as shown in Fig. 9j, k), and finally, when a_e/D = 1 (full-immersion), the two lines coincide with each other, as shown in Fig. 9l.

The reasons for this phenomenon are explained as follows: for the same spindle rotation directions, the feed directions of up-milling and down-milling are different, as a result, for the partial-immersion condition, the start angle and the exit angle of cutter tooth for these two operations are also different, leading to different SLDs; for the full immersion condition (a_e/D = 1), the start angle and the exit angle of cutter tooth for up-milling and down-milling are the same; therefore, the SLDs of these two operations are identical.

In order to investigate the influence of regenerative effect, mode coupling effect, and process damping on the stability prediction of actual milling, a series of experiments (up-milling and down-milling operations) are carried out in the following section.

4.2 Experimental validation

It is clear from the above analysis that the regenerative effect, mode coupling, and process damping have some influences on the stability boundaries. To verify the effectiveness of the proposed dynamical model and indicate to what extend does the multiple factors coupling effects (the regenerative effect, mode coupling, and process damping) influence the stability boundaries, a series of milling experiments are conducted. The experiment is conducted on a five-axis high-speed machining center, of which the maximal spindle speed is 18,000 r/min. As discussed by Balachandran et al. [19–21], linear dynamics models can provide quite accurate stability predictions for high-immersion milling operations, so the experiment is carried out with full-immersion. The workpiece is aluminum alloy block. The cutter is a carbide alloy end tool with three flutes. The tool parameters are listed in Table 2.

4.2.1 Determination of the cutting force coefficients

The cutting force coefficients are the foundation of chatter prediction. In this paper, the tangential cutting force coefficient K_t and the normal linear cutting force coefficient K_n were obtained by slot-milling experiment.

During the experiment, the 9257B type three-component Kisler dynamometer is applied to collect the force signals of X, Y, and Z directions. All workpieces used in this paper are 130 × 50 × 15 mm^3 in size and made

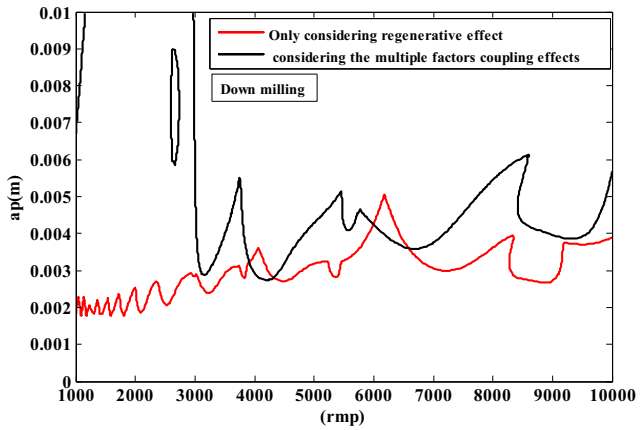

Fig. 8 The SLD for down-milling (1/2 immersion) by considering the regenerative effect (the red line) and simultaneously considering the regenerative effect, mode coupling, and process damping (the black line)

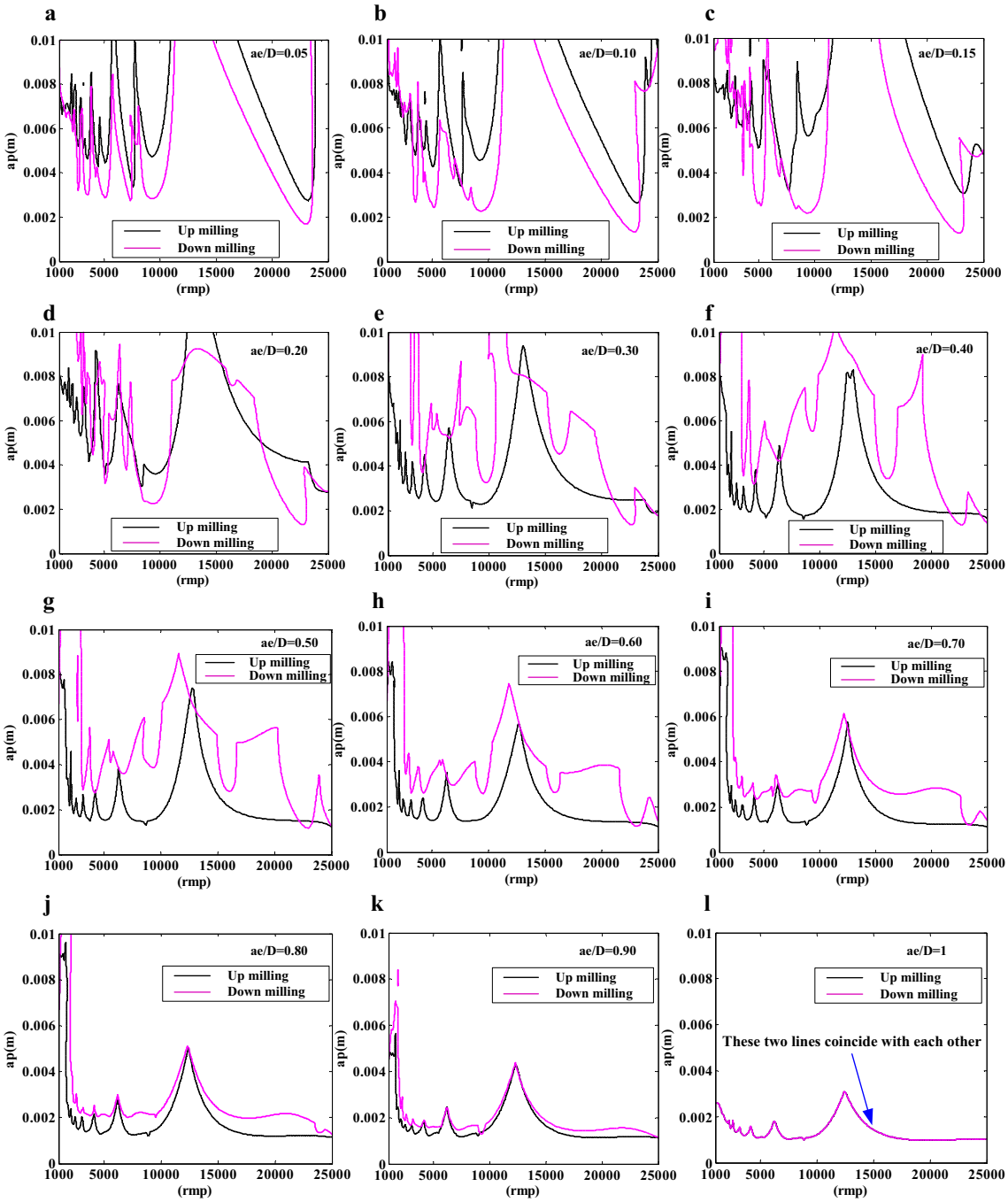

Fig. 9 The simulation results for up and down-milling operations with different radial immersion ratios (a_e/D)

of aluminum alloy. During the experiment, the spindle speed, the axial depth of cut, and the radial width of cut are constant; the feed per tooth is varied linearly. As discussed by Wang et al. [51], the cutting force coefficients are only related to the tool-workpiece material couple and the tool geometrical parameters, and not affected by the milling parameters, so it is relatively free in the aspect of milling parameter selection.

Table 2 The parameters of the tool

Diameter (mm)	Number of flutes	Flute length (mm)	Cutter length (mm)	Helix angle (deg.)
10	3	45	100	45

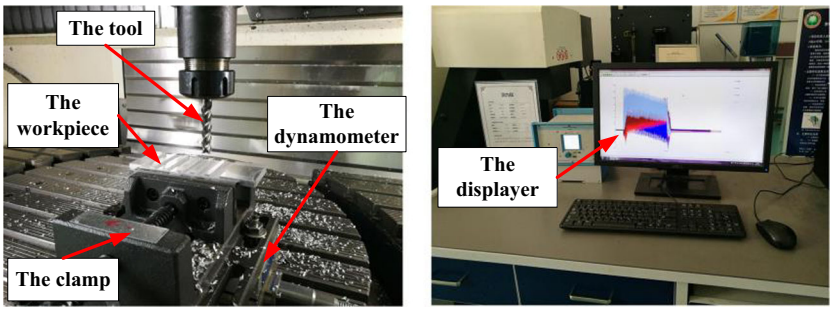

Fig. 10 The experiment site of determining the cutting force coefficients

The milling parameters are selected as list: fixed spindle speed of 2000 rpm, axial depth of cut 2 mm, radial width of cut 10 mm, the feed per tooth is varied linearly, i.e., 0.02, 0.04, 0.06, 0.08, and 0.10 mm, respectively. The experiment site is shown in Fig. 10. The average milling forces in the X and Y direction with each combination of milling parameters are listed in Table 3. In Table 3, n, a_p, a_e, a_f, $\overline{F}x$, $\overline{F}y$ denote the spindle, axial depth of cut, radial width of cut, feed per tooth, the average force in X direction, and the average force in Y direction, respectively.

The linear expressions of average milling force as a function of feed per tooth are shown as Eq. (92)–(93). Figure 11 shows the linear fitting graphs of the average milling force in the direction of X and Y, respectively.

$$fx = 486.05af + 29.809 \tag{92}$$

$$fy = 1336.5af + 34.906 \tag{93}$$

Based on the average cutting force model [51], the milling force coefficients can be obtained, as shown in the following: $Kt = 891N/mm^2$, $Kn = 324N/mm^2$.

4.2.2 Determination of the modal parameters

The modal test experiment is performed to identify the modal parameters of the cutting system. An acceleration sensor of YD67 type with a sensitivity of 0.38 PC/(m•s^{-2}) and a frequency range between 1 and 18,000 HZ is adhered to the selected position of the tool by plasticine in order to obtain response signals. A MSC-1 impact hammer with a 500 kgf sensor is utilized to knock the tool with the aim of generating stimulus signals. A DLF-3 type two-channel charge amplifier with an attenuation rate greater than 140 Db/oct is used to amplify the stimulus signals. Finally, the stimulus signals are acquired by an AD8304 type four-channel data acquisition unit and analyzed by DynaCut software.

The flow chart of data acquisition, arrangement scheme of the acceleration sensor, and the experiment facilities are shown in Fig. 12.

To eliminate the accidental error, the modal impact testing is conducted five times and the average valve of each modal parameter is taken as the final result. The average modal parameters (first mode) are shown in Table 4. It is clear from Table 4 that there are coupling terms in the direction of X-Y.

Table 3 Average milling force in the X and Y direction

n (rpm)	a_p (mm)	a_e (mm)	a_f (mm)	$\overline{F}x$ (N)	$\overline{F}y$ (N)
2000	2	10	0.02	37.9	59.32
2000	2	10	0.04	50.76	90.96
2000	2	10	0.06	61.22	116.5
2000	2	10	0.08	66.19	140.5
2000	2	10	0.10	78.79	168.2

4.2.3 Experimental results and analysis

Tool wear is inevitable and appropriate wear land width can improve milling stability. In this paper, the proposed dynamical model is an integrated model which simultaneously consider the multiple factor coupling effect, i.e., regenerative effect, mode coupling, and process damping. As discussed in

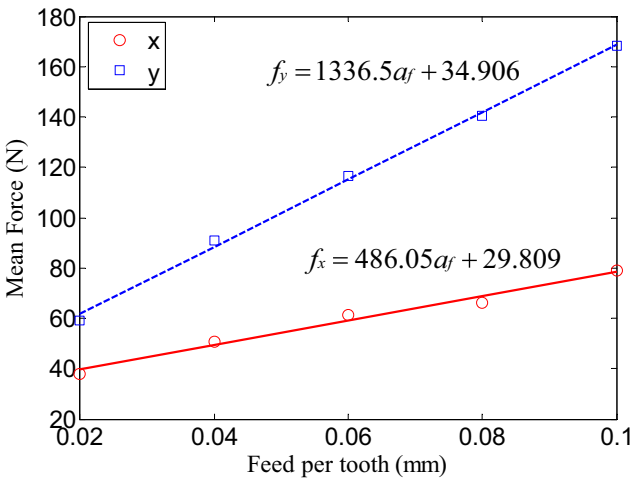

Fig. 11 The linear fitting graphs of the average milling force in X and Y directions

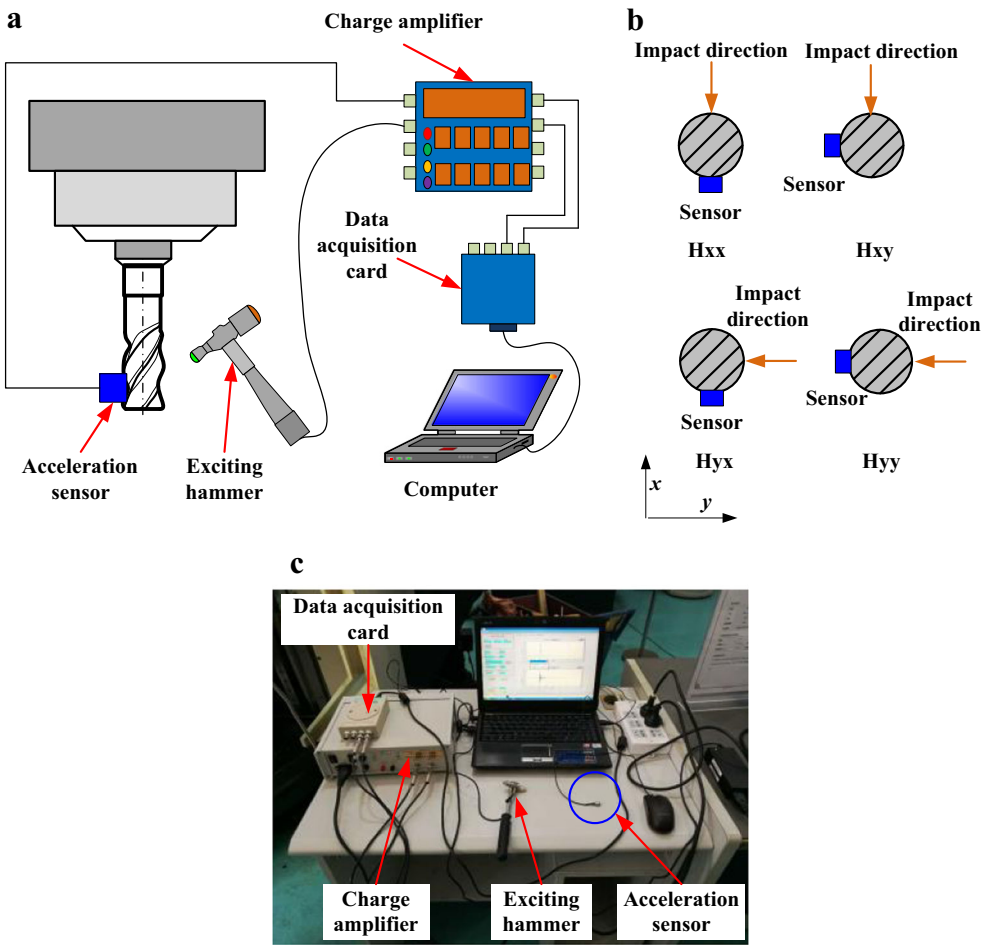

Fig. 12 The flow chart of modal test. **a** The data collection system, **b** the arrangement scheme of the acceleration sensor, **c** the experimental facilities

Sect. 2.2, process damping is related to the tool wear, so the wear land width should be determined if we want to take process damping into account. The geometrical parameters of the tool are shown in Table 2. The wear land width of the flank surface of cutting tool is measured by KEYENCE laser confocal microscope (VK-X100). As shown in Fig. 13, the wear land width value for one of the cutting edge is 39.7 μm. The wear land width values for other two cutting edges are 39.9 and 40.1 μm, respectively. In this article, to calculate the process damping, the wear land width is determined as an average value 40 μm.

Table 4 The modal parameters

Direction	Frequency (Hz)	Damping	Mass (kg)
Xx	1419.30	0.02115	0.42825
Xy	1398.44	0.03318	0.10542
Yx	1459.68	0.02641	0.13261
Yy	1610.1	0.06871	0.36582

According to the parameters of Table 4 and $Kt = 891N/mm^2$, $Kn = 324N/mm^2$, the SLD can be obtained by the updated full discretization method (FDM). In this section, the stability charts are calculated over a 200×200 sized grid of

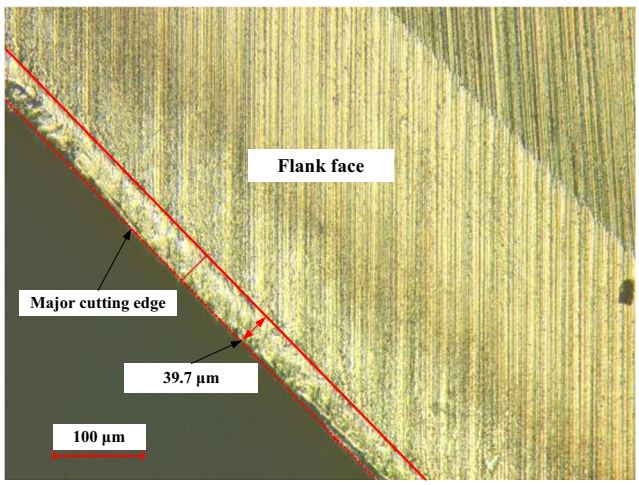

Fig. 13 The wear land of the tool

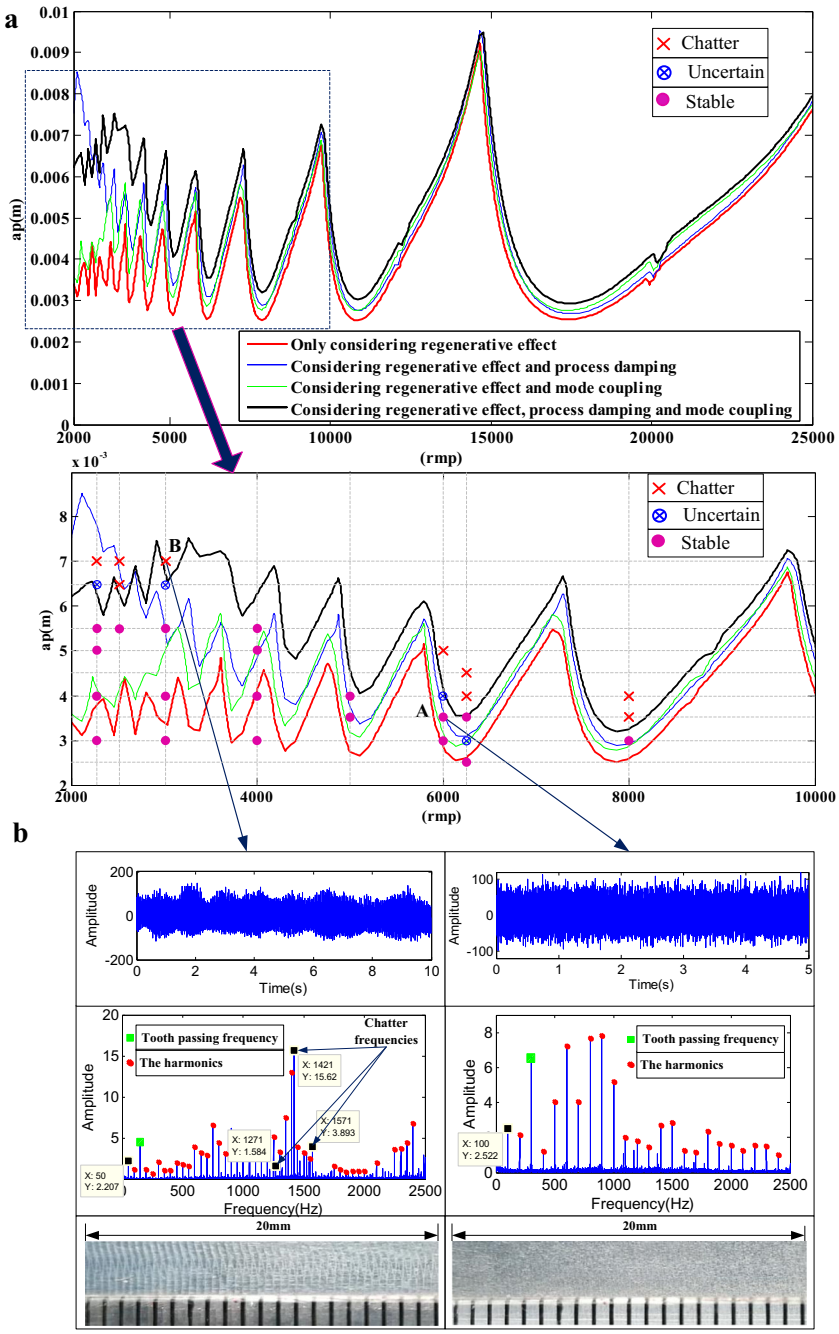

Fig. 14 **a** The stability lobe diagrams of down-milling operation ($a_e/D = 1$). **b** The time-domain signal, frequency spectrum, and surface topography of different milling states

spindle speed Ω and the axial depth of cut a_p. The time intervals $m = 50$ and the axial depth of cut ranging from 0 to 0.010 m, the spindle speed ranging from 2×10^3 to 25×10^3 rpm. The milling style is down-milling and up-milling operations, respectively. The SLDs (for down-milling) which are based on different milling dynamical models are shown in Fig. 14. In Fig. 14a, the red line represents the SLD which is obtained by only considering regenerative effect; the blue line represents the SLD which is obtained by considering regenerative effect and process damping; the green line represents the SLD which is obtained by considering regenerative effect and mode coupling; the black line represents the SLD which is obtained by considering regenerative effect, mode coupling effect, and process damping.

It is clear from Fig. 14a that when the regenerative effect and process damping are considered, there are more stability region in low spindle speed region than the SLD which is obtained only by considering the regenerative effect, while in high spindle speed region, the SLDs are almost coincident, which means that process damping has no obvious influence

Table 5 The cutting parameters

No.	Spindle speed (r/min)	Axial depth (mm)	Radial depth (mm)	Feed per tooth (mm)
1	2250	3.0	10	0.05
2	2250	4.0	10	0.05
3	2250	5.0	10	0.05
4	2250	5.5	10	0.05
5	2250	6.5	10	0.05
6	2250	7.0	10	0.05
7	2500	5.5	10	0.05
8	2500	6.5	10	0.05
9	2500	7.0	10	0.05
10	3000	3.0	10	0.05
11	3000	4.0	10	0.05
12	3000	5.5	10	0.05
13	3000	6.5	10	0.05
14	3000	7.0	10	0.05
15	4000	3.0	10	0.05
16	4000	4.0	10	0.05
17	4000	5.0	10	0.05
18	4000	5.5	10	0.05
19	5000	3.5	10	0.05
20	5000	4.0	10	0.05
21	6000	3.0	10	0.05
22	6000	3.5	10	0.05
23	6000	4.0	10	0.05
24	6000	5.0	10	0.05
25	6250	2.5	10	0.05
26	6250	3.0	10	0.05
27	6250	3.5	10	0.05
28	6250	4.0	10	0.05
29	6250	4.5	10	0.05
30	8000	3.0	10	0.05
31	8000	3.5	10	0.05
32	8000	4.0	10	0.05

on the SLD when at high spindle speed cutting situation; when regenerative effect and mode coupling effect are considered, the SLD also is changed compared with the SLD which is obtained by only considering the regenerative effect; when the multiple factor coupling effect (i.e., regenerative effect, mode coupling effect, and process damping) is considered, there are more stability region in low spindle speed region than the SLD which is obtained by considering regenerative

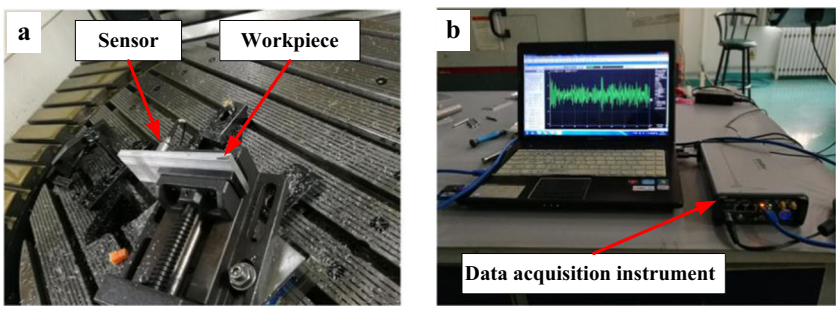

Fig. 15 Acquisition of the vibration acceleration signal. **a** Assignment of the acceleration sensor. **b** The signal acquisition system

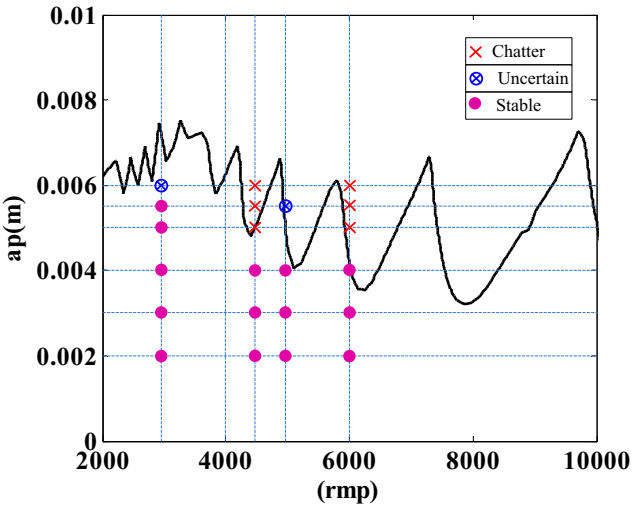

Fig. 16 SLD obtained by considering regenerative effect, mode coupling effect, and process damping for up-milling operation and the experiment results

effect and mode coupling effect. The milling experiment (flank milling with full-immersion) is performed to verify the stability prediction of the proposed method. The milling style is down-milling. The cutting parameters are listed in Table 5.

In order to identify the milling state, the vibration acceleration signal is recorded by an INV9822 type acceleration sensor with the sensitivity of 10.355 mV/ms^{-2}; the INV3062T type four-channel data acquisition instrument is used to collect the signals. The sampling frequency is 12.8×10^3 Hz. The assignment of the sensor in the signal acquisition experiment is shown in Fig. 15. The experiment results almost agree with the SLD which is obtained by considering the multiple factor coupling effect (as shown in Fig. 14a). In Fig. 14a, point A (6000 rpm, 0.0035 m) is stable and point B (3000 rpm, 0.007 m) is unstable. The frequency spectrum and the workpiece surface topography of point A and point B are shown in Fig. 14b. It is clear from Fig. 14b that the frequency spectrum of the vibration acceleration signal of point A (6000 rpm, 0.0035 m) basically consists of the fundamental frequency (6000/60 = 100 Hz), the tooth passing frequency (6000/60 × 3 = 300 Hz), and its harmonics. In addition, the surface of the workpiece is relatively smooth, which means that the cutting process is stable.

However, at point B (3000 rpm, 0.007 m), the frequency spectrum shows that there are strong chatter frequencies (1271, 1421, and 1571 Hz) in the frequency band; the difference of the chatter frequencies is 150, which equals to the tooth passing frequency (3000/60 × 3 = 150 Hz). And there are obvious chatter marks on the workpiece surface. The experiment results show that the SLD which is obtained by the milling dynamical equation (considering the regenerative effect, mode coupling, and process damping) more agrees with the actual milling conditions.

For up-milling operation, the SLD which is obtained by considering regenerative effect, mode coupling effect, and process damping is shown in Fig. 16. Also, the milling experiment (full-immersion) is carried out to verify the accuracy of the SLD. It is clear from Fig. 16 that the SLD agrees with the actual milling conditions, which indicates that the new milling dynamical equation is effective in the aspect of stability prediction.

5 Conclusions and future works

Milling is a complicated cutting process which involves in a variety of complex factors. Milling chatter which is related to the regenerative effect, mode coupling, and process damping effect always causes bad effects on the workpiece and the tool. In order to avoid chatter, suitable machining parameters should be selected during machining process. For purposes of obtaining the stability lobe diagrams of milling process, the dynamical model of milling which by considering the regenerative effect, mode coupling effect, and process damping is established, based on which the new SLD is obtained. The experiment results show that the SLD which is obtained by considering the multiple factor coupling effect (i.e., regenerative effect, mode coupling effect, and process damping) more agrees with the actual milling conditions.

Here, some conclusions are summarized:

(1) A new milling dynamical equation which simultaneously considering the regenerative effect, mode coupling effect, and process damping is established.
(2) The experiment results show that the mode coupling effect and process damping have great influence on the prediction of milling stability. The SLD which is obtained by the new milling dynamical equation (considering the regenerative effect, mode coupling, and process damping) is more accurate than that which obtained by the traditional dynamical equation (considering the regenerative effect).
(3) Milling is a complicated dynamic material removal process, which will cause the change of modal parameters, how to establish a more accurate mathematical model by considering the dynamic impact factors will be the research direction for our future works.

Acknowledgements This work is jointly supported by the National Natural Science Foundation of China (Grant No. 51375055 and 51575055); The High-end CNC machine tools and basic manufacturing equipment Science and Technology Major Project of China (Grant No. 2015ZX04001002); Junior Fellowships for CAST Advanced Innovation Program (DXB-ZKQN-2016-003).

Appendix. MATLAB codes for the simulated SLD of up-milling (Fig. 7) by considering the regenerative effect, mode coupling and process damping

```
close all,clear all,clc
N=3;            %number of teeth
Kt=7e8;         %tangential cutting force coefficient(N/m2)
Kn=0.49e8;      %normal cutting force coefficient(N/m2)
mu=0.3;         %coulomb friction coefficient
%modal mass (Kg)
m_tx=0.39;m_txy=0.234*1;m_tyx=0.192*1;m_ty=0.32;
%modal damping
Cx=115.29;Cxy=69.174*1;Cyx=57.21*1;Cy=95.35;
%modal stiffness
Kx=5.6*10^(6);Kxy=3.36*10^(6)*1;Kyx=3.42*10^(6)*1;
Ky=5.7*10^(6);
%%
aD=0.5;
up_or_down=1;
if up_or_down==1
   fist=0;
   fiex=acos(1-2*aD);
elseif up_or_down==-1
   fist=acos(2*aD-1);
   fiex=pi;
end
stx=200;sty=200;w_st=0e-3;w_fi=10e-3;o_st=1e3;o_fi=10e3;
m=50;
D=zeros(4*m+4,4*m+4);
vlow=ones(4*m,1);
D=D+diag(vlow,-4);
for i=1:m+1
   dtr=2*pi/N/m;
   hxx1(i)=0; hxy1(i)=0;hyx1(i)=0; hyy1(i)=0;
   hpxx(i)=0; hpxy(i)=0; hpyx(i)=0;hpyy(i)=0;
  for j=1:N
 fi1=i*dtr+(j-1)*2*pi/N;
      if (fi1>=fist)*(fi1<=fiex)
         g=1;
      else
         g=0;
      end
      hxx1(i)=hxx1(i)+g*(Kt*cos(fi1)+Kn*sin(fi1))*sin(fi1);
      hxy1(i)=hxy1(i)+g*(Kt*cos(fi1)+Kn*sin(fi1))*cos(fi1);
      hyx1(i)=hyx1(i)+g*(-Kt*sin(fi1)+Kn*cos(fi1))*sin(fi1);
      hyy1(i)=hyy1(i)+g*(-Kt*sin(fi1)+Kn*cos(fi1))*cos(fi1);
      %%
      hpxx(i)=hpxx(i)+g*sin(fi1)*(sin(fi1)+mu*cos(fi1));
      hpxy(i)=hpxy(i)+g*cos(fi1)*(sin(fi1)+mu*cos(fi1));
      hpyx(i)=hpyx(i)+g*sin(fi1)*(cos(fi1)-mu*sin(fi1));
      hpyy(i)=hpyy(i)+g*cos(fi1)*(cos(fi1)-mu*sin(fi1));
   end
end
%%
k1=-m_ty*Kx/(m_tx*m_ty-m_txy*m_tyx)+m_txy*Kyx/
(m_tx*m_ty-m_txy*m_tyx);
k2=-m_ty*Kxy/(m_tx*m_ty-m_txy*m_tyx)+m_txy*Ky/
(m_tx*m_ty-m_txy*m_tyx);
k3=m_tyx*Kx/(m_tx*m_ty-m_txy*m_tyx)-m_tx*Kyx/
(m_tx*m_ty-m_txy*m_tyx);
k4=m_tyx*Kxy/(m_tx*m_ty-m_txy*m_tyx)-m_tx*Ky/
(m_tx*m_ty-m_txy*m_tyx);
m1=-m_ty*Cx/(m_tx*m_ty-m_txy*m_tyx)+m_txy*Cyx/
(m_tx*m_ty-m_txy*m_tyx);
m2=-m_ty*Cxy/(m_tx*m_ty-m_txy*m_tyx)+m_txy*Cy/
(m_tx*m_ty-m_txy*m_tyx);
m3=m_tyx*Cx/(m_tx*m_ty-m_txy*m_tyx)-m_tx*Cyx/
(m_tx*m_ty-m_txy*m_tyx);
m4=m_tyx*Cxy/(m_tx*m_ty-m_txy*m_tyx)-m_tx*Cy/
(m_tx*m_ty-m_txy*m_tyx);
A0=[0 0 1 0;0 0 0 1;k1 k2 m1 m2;k3 k4 m3 m4];
%%
I=eye(size(A0));
invA0=inv(A0);
for x=1:stx+1
o=o_st+(x-1)*(o_fi-o_st)/stx;
tau=60/o/N;
dt=tau/m;
Fi0=invA0*(expm(A0*dt)-I);
Fi1=invA0*(Fi0-dt*I);
Fi2=invA0*(2*Fi1-dt*dt*I);
Fi3=invA0*(3*Fi2-dt*dt*dt*I);
Fi4=invA0*(4*Fi3-dt*dt*dt*dt*I);
G11_1=-(A0/dt^3-2*I/dt^4)*Fi4+(2*A0/dt^2-5*I/dt^3)*Fi3+(3*I/dt^2-A0/dt)*Fi2;
G12_1=(A0/dt^3-2*I/dt^4)*Fi4+(3*I/dt^3-A0/dt^2)*Fi3;
G13_1=Fi1/dt+A0*Fi2/dt+(-2*A0/(dt^2)-3*I/(dt^3))*Fi3+(2*I/(dt^4)+A0/dt^3)*Fi4;
G14_1=(5*I/dt^3+3*A0/dt^2)*Fi3+Fi0+(A0-I/dt)*Fi1+(-3*A0/dt-3*I/dt^2)*Fi2-(2*I/dt^4+A0/dt^3)*Fi4;
G15=1/(6*dt*dt*dt*dt)*Fi4-1/(2*dt*dt*dt)*Fi3+1/(3*dt*dt)*Fi2;
G16=-1/(6*dt*dt*dt*dt)*Fi4+2/(3*dt*dt*dt)*Fi3-5/(6*dt*dt)*Fi2+1/(3*dt)*Fi1;
G17=-1/(2*dt*dt*dt*dt)*Fi4+2/(dt*dt*dt)*Fi3-3/(2*dt*dt)*Fi2;
G18=1/(2*dt*dt*dt*dt)*Fi4-5/(2*dt*dt*dt)*Fi3+7/(2*dt*dt)*Fi2-3/(2*dt)*Fi1;
%%
G21=1/(2*dt*dt*dt*dt)*Fi4-5/(2*dt*dt*dt)*Fi3+3/(dt*dt)*Fi2;
G22=-1/(2*dt*dt*dt*dt)*Fi4+3/(dt*dt*dt)*Fi3-11/(2*dt*dt)*Fi2+3/(dt)*Fi1;
G25=-1/(6*dt*dt*dt*dt)*Fi4+1/(dt*dt*dt)*Fi3-11/(6*dt*dt)*Fi2+1/dt*Fi1;
G26=1/(6*dt*dt*dt*dt)*Fi4-7/(6*dt*dt*dt)*Fi3+17/(6*dt*dt)*Fi2-17/(6*dt)*Fi1+Fi0;
%%
   for y=1:sty+1
      w=w_st+(y-1)*(w_fi-w_st)/sty;
      Fi=eye(4*m+4,4*m+4);
      for i=1:m
    Ksp=1.5*10^14*1;
    W=0.00008;                  %Wear land width of the tool (m)
    V=pi*0.0254*o/60;
    Cep=Ksp*w*W^2/(4*V);
%%
O1_1=-m_ty*w*hxx1(i)/(m_tx*m_ty-m_txy*m_tyx)+m_txy*w*hyx1(i)/(m_tx*m_ty-m_txy*m_tyx);
O2_1=-m_ty*w*hxy1(i)/(m_tx*m_ty-m_txy*m_tyx)+m_txy*w*hyy1(i)/(m_tx*m_ty-m_txy*m_tyx);
O3_1=m_tyx*w*hxx1(i)/(m_tx*m_ty-m_txy*m_tyx)-m_tx*w*hyx1(i)/(m_tx*m_ty-m_txy*m_tyx);
O4_1=m_tyx*w*hxy1(i)/(m_tx*m_ty-m_txy*m_tyx)-m_tx*w*hyy1(i)/(m_tx*m_ty-m_txy*m_tyx);
O1_2=-m_ty*w*hxx1(i+1)/(m_tx*m_ty-m_txy*m_tyx)+m_txy*w*hyx1(i+1)/(m_tx*m_ty-m_txy*m_tyx);
O2_2=-m_ty*w*hxy1(i+1)/(m_tx*m_ty-m_txy*m_tyx)+m_txy*w*hyy1(i+1)/(m_tx*m_ty-m_txy*m_tyx);
O3_2=m_tyx*w*hxx1(i+1)/(m_tx*m_ty-m_txy*m_tyx)-m_tx*w*hyx1(i+1)/(m_tx*m_ty-m_txy*m_tyx);
O4_2=m_tyx*w*hxy1(i+1)/(m_tx*m_ty-m_txy*m_tyx)-m_tx*w*hyy1(i+1)/(m_tx*m_ty-m_txy*m_tyx);
%%
f1_1=-m_ty*hpxx(i)/(m_tx*m_ty-m_txy*m_tyx)+m_txy*hpyx(i)/(m_tx*m_ty-m_txy*m_tyx);
f2_1=-m_ty*hpxy(i)/(m_tx*m_ty-m_txy*m_tyx)+m_txy*hpyy(i)/(m_tx*m_ty-m_txy*m_tyx);
f3_1=m_tyx*hpxx(i)/(m_tx*m_ty-m_txy*m_tyx)-m_tx*hpyx(i)/(m_tx*m_ty-m_txy*m_tyx);
f4_1=m_tyx*hpxy(i)/(m_tx*m_ty-m_txy*m_tyx)-m_tx*hpyy(i)/(m_tx*m_ty-m_txy*m_tyx);
f1_2=-m_ty*hpxx(i+1)/(m_tx*m_ty-m_txy*m_tyx)+m_txy*hpyx(i+1)/(m_tx*m_ty-m_txy*m_tyx);
f2_2=-m_ty*hpxy(i+1)/(m_tx*m_ty-m_txy*m_tyx)+m_txy*hpyy(i+1)/(m_tx*m_ty-m_txy*m_tyx);
f3_2=m_tyx*hpxx(i+1)/(m_tx*m_ty-m_txy*m_tyx)-m_tx*hpyx(i+1)/(m_tx*m_ty-m_txy*m_tyx);
f4_2=m_tyx*hpxy(i+1)/(m_tx*m_ty-m_txy*m_tyx)-m_tx*hpyy(i+1)/(m_tx*m_ty-m_txy*m_tyx);
R0k=[0 0 0 0;0 0 0 0;O1_1 O2_1 f1_1*Cep f2_1*Cep;O3_1 O4_1 f3_1*Cep f4_1*Cep];
R1k=[0 0 0 0;0 0 0 0;O1_2 O2_2 f1_2*Cep f2_2*Cep;O3_2 O4_2 f3_2*Cep f4_2*Cep];
L0k=[0 0 0 0;0 0 0 0;O1_1 O2_1 0 0;O3_1 O4_1 0 0];
L1k=[0 0 0 0;0 0 0 0;O1_2 O2_2 0 0;O3_2 O4_2 0 0];
    G11_2=-R1k/dt^3*Fi4+2*R1k/dt^2*Fi3-R1k/dt*Fi2;
    G12_2=R1k/dt^3*Fi4-R1k/dt^2*Fi3;
    G13_2=R0k/dt^3*Fi4-2*R0k/dt^2*Fi3+R0k/dt*Fi2;
    G14_2=-R0k/dt^3*Fi4+3*R0k/dt^2*Fi3-3*R0k/dt*Fi2+R0k*Fi1;
    G11=G11_1+G11_2;G12=G12_1+G12_2; G13=G13_1+G13_2;G14=G14_1+G14_2;
    G19=-L1k/dt^3*Fi4+L1k/dt^2*Fi3;
    G20=L1k/dt^3*Fi4-2*L1k/dt^2*Fi3+L1k/dt*Fi2;
    G23=-L0k/dt^3*Fi4+2*L0k/dt^2*Fi3-L0k/dt*Fi2;
    G24=L0k/dt^3*Fi4-3*L0k/dt^2*Fi3+3*L0k/dt*Fi2-L0k*Fi1;
        Qj=(I-(G11*R0k+G12*R1k));
        Hj=G14*R0k+G13*R1k+expm(A0*dt);
        Hjr1=-G15*L1k-G16*L0k;
        Hjr2=-G17*L1k-G18*L0k;
        Hjr3=(G19*R1k+G20*R0k)-(G21*L1k+G22*L0k);
        Hjr4=(G23*R1k+G24*R0k)-(G25*L1k+G26*L0k);
        invQ=inv(Qj);
        M11=invQ*Hjr1;
        M12=invQ*Hjr2;
        M13=invQ*Hjr3;
        M14=invQ*Hjr4;
        D(1:4,1:4)=invQ*Hj;
        D(1:4,4*m-11:4*m-8)=M11(1:4,1:4);
        D(1:4,4*m-7:4*m-4)=M12(1:4,1:4);
        D(1:4,4*m-3:4*m)=M13(1:4,1:4);
        D(1:4,4*m+1:4*m+4)=M14(1:4,1:4);
        Fi=D*Fi;
      end
      ss(x,y)=o;
      dc(x,y)=w;
      ei(x,y)=max(abs(eig(Fi)));
   end
   stx+1-x
end
figure;
contour(ss,dc,ei,[1,1],'k'),xlabel('(rmp)'),ylabel('ap(m)')
```

References

1. Faassen RPH, van de Wouw N, Oosterling JAJ, Nijmeijer H (2003) Prediction of regenerative chatter by modelling and analysis of high-speed milling. Int J Mach Tools Manuf 43(14):1437–1446. https://doi.org/10.1016/S0890-6955(03)00171-8
2. Tlusty J, Polacek M (1963) The stability of machine tools against self excited vibrations in machining. ASME Production Engineering Research Conference, Pittsburgh, PA, pp 465–474
3. Tunc T, Budak E (2013) Identification and modeling of process damping in milling. J Manuf Sci Eng 135(2):1–12. https://doi.org/10.1115/1.4023708
4. Liu XB, Vlajic N, Long XH, Meng G, Balachandran B (2014) Multiple regenerative effects in cutting process and nonlinear oscillations. Int J Dynam Control 2(1):86–101. https://doi.org/10.1007/s40435-014-0078-5
5. Balachandran B (2001) Nonlinear dynamics of milling processes. Philos Trans R Soc Lond A 359(1781):793–819. https://doi.org/10.1098/rsta.2000.0755
6. Richard T, Germay C, Detournay E (2004) Self-excited stick-slip oscillations of drill bits. C R Mec 332(8):619–626. https://doi.org/10.1016/j.crme.2004.01.016
7. Quintana G, Ciurana J (2011) Chatter in machining processes: a review. Int J Mach Tools Manuf 51(5):363–376. https://doi.org/10.1016/j.ijmachtools.2011.01.001
8. Altintas Y, Budak E (1995) Analytical prediction of stability lobes in milling. CIRP Ann-Manuf Technol 44(1):357–362. https://doi.org/10.1016/S0007-8506(07)62342-7
9. Merdol SD, Altintas Y (2004) Multi frequency solution of chatter stability for low immersion milling. J Manuf Sci Eng-Trans ASME 126(3):459–466. https://doi.org/10.1115/1.1765139
10. Minis I, Yanushevsky R (1993) A new theoretical approach for the prediction of machine tool chatter in milling. J Eng Ind 115(1):1–8. https://doi.org/10.1115/1.2901633
11. Insperger T, Stépán G (2004) Updated semi-discretization method for periodic delay-differential equations with discrete delay. Int J Numer Methods Eng 61(1):117–141. https://doi.org/10.1002/nme.1061
12. Ding Y, Zhu LM, Zhang XJ, Ding H (2010) A full-discretization method for prediction of milling stability. Int J Mach Tools Manuf 50(5):502–509. https://doi.org/10.1016/j.ijmachtools.2010.01.003
13. Yan ZH, Wang XB, Liu ZB, Wang DQ, Jiao L, Ji YJ (2017) Third-order updated full-discretization method for milling stability prediction. Int J Adv Manuf Technol 92(5–8):2299–2309. https://doi.org/10.1007/s00170-017-0243-z
14. Yan ZH, Wang XB, Liu ZB, Wang DQ, Ji YJ, Jiao L (2017) Orthogonal polynomial approximation method for stability prediction in milling. Int J Adv Manuf Technol 91(9–12):4313–4330. https://doi.org/10.1007/s00170-017-0067-x
15. Zhou K, Feng PF, Xu C, Zhang JF, Wu ZJ (2017) High-order full-discretization methods for milling stability prediction by interpolating the delay term of time-delayed differential equations. Int J Adv Manuf Technol 93(5–8):2201–2214. https://doi.org/10.1007/s00170-017-0692-4
16. Ding Y, Zhu LM, Zhang XJ, Ding H (2011) Numerical integration method for prediction of milling stability. J Manuf Sci Eng 133(3):1–9. https://doi.org/10.1115/1.4004136
17. Ding Y, Zhu LM, Zhang XJ, Ding H (2011) Milling stability analysis using the spectral method. Sci China Technol Sci 54(12):3130–3136. https://doi.org/10.1007/s11431-011-4611-x
18. Zhang Z, Li HG, Meng G, Liu C (2015) A novel approach for the prediction of the milling stability based on the Simpson method. Int J Mach Tools Manuf 99:43–47. https://doi.org/10.1016/j.ijmachtools.2015.09.002
19. Balachandran B, Gilsinn D (2005) Non-linear oscillations of milling. Math Comput Model Dyn Syst 11(3):273–290. https://doi.org/10.1080/13873950500076479
20. Zhao MX, Balachandran B (2001) Dynamics and stability of milling process. Int J Solids Struct 38(10–13):2233–2248. https://doi.org/10.1016/S0020-7683(00)00164-5
21. Balachandran B, Zhao MX (2000) A mechanics based model for study of dynamics of milling operations. Meccanica 35(2):89–109. https://doi.org/10.1023/A:1004887301926
22. Zhang XJ, Xiong CH, Ding Y, Feng MJ, Xiong YL (2012) Milling stability analysis with simultaneously considering the structural mode coupling effect and regenerative effect. Int J Mach Tools Manuf 53(1):127–140. https://doi.org/10.1016/j.ijmachtools.2011.10.004
23. Gasparetto A (1998) A system theory approach to mode coupling chatter in machining. J Dyn Sys, Meas, Control 120(4):545–547. https://doi.org/10.1115/1.2801501
24. Gasparetto A (2001) Eigenvalue analysis of mode-coupling chatter for machine-tool stabilization. J Vib Control 7(2):181–197. https://doi.org/10.1177/107754630100700203
25. Gallina P, Trevisani A (2003) On the stabilizing and destabilizing effects of damping in wood cutting machines. Int J Mach Tools Manuf 43(9):955–964. https://doi.org/10.1016/S0890-6955(03)00061-0
26. Hoffmann N, Gaul L (2003) Effects of damping on mode-coupling in stability in friction induced oscillations. ZAMM-J Appl Math Mech 83(8):524–534. https://doi.org/10.1002/zamm.200310022
27. Pan ZX, Zhang H, Zhu ZQ, Wang JJ (2006) Chatter analysis of robotic machining process. J Mater Process Technol 173(3):301–309. https://doi.org/10.1016/j.jmatprotec.2005.11.033
28. Iturrospe A, Atxa V, Abete JM (2007) State-space analysis of mode-coupling in orthogonal metal cutting under wave regeneration. Int J Mach Tools Manuf 47(10):1583–1592. https://doi.org/10.1016/j.ijmachtools.2006.11.005
29. Li ZY, Jiang SL, Sun YW (2017) Chatter stability and surface location error predictions in milling with mode coupling and process damping. Proc IMechE Part B: J Eng Manuf:1–13. https://doi.org/10.1177/0954405417708225
30. Wallace PW, Andrew C (1965) Machining forces: some effects of tool vibration. J Mech Eng Sci 7(2):152–162. https://doi.org/10.1243/JMES_JOUR_1965_007_023_02
31. Ahmadi K, Altintas Y (2014) Identification of machining process damping using output-only modal analysis. J Manuf Sci Eng-Trans ASME 136(5):051017. https://doi.org/10.1115/1.4027676
32. Ahmadi K, Ismail F (2012) Stability lobes in milling including process damping and utilizing multi-frequency and semi-discretization methods. Int J Mach Tools Manuf 54-55:46–54. https://doi.org/10.1016/j.ijmachtools.2011.11.007
33. Huang CY, Wang JJJ (2007) Mechanistic modeling of process damping in peripheral milling. J Manuf Sci Eng 129(1):12–20. https://doi.org/10.1115/1.2335857
34. Ahmadi K, Ismail F (2011) Analytical stability lobes including nonlinear process damping effect on machining chatter. Int J Mach Tools Manuf 51(4):296–308. https://doi.org/10.1016/j.ijmachtools.2010.12.008
35. Ahmadi K (2017) Analytical investigation of machining chatter by considering the nonlinearity of process damping. J Sound Vibr 393:252–264. https://doi.org/10.1016/j.jsv.2017.01.006
36. Malekian M, Park SS, Jun MBG (2009) Modeling of dynamic micro-milling cutting forces. Int J Mach Tools Manuf 49(7–8):586–598. https://doi.org/10.1016/j.ijmachtools.2009.02.006

37. Lu YA, Ding Y, Zhu LM (2017) Dynamics and stability prediction of five-Axis flat-end milling. J Manuf Sci Eng 139(6):1–11. https://doi.org/10.1115/1.4035422
38. Wu DW (1989) A new approach of formulating the transfer function for dynamic cutting process. J Eng Ind 111(1):37–47. https://doi.org/10.1115/1.3188730
39. Kurata Y, Merdol SD, Altintas Y, Suzuki N, Shamoto E (2010) Chatter stability in turning and milling within process identified process damping. J Adv Mech Design, Syst, Manuf 4(6):1107–1118. https://doi.org/10.1299/jamdsm.4.1107
40. Chiou YS, Chung ES, Liang SY (1995) Analysis of tool wear effect on chatter stability in turning. Int J Mech Sci 37(4):391–404. https://doi.org/10.1016/0020-7403(94)00070-Z
41. Ji YJ, Wang XB, Liu ZB, Wang HJ, Yan ZH (2018) An updated full-discretization milling stability prediction method based on the higher order Hermite-Newton interpolation polynomial. Int J Adv Manuf Technol 95(5–8):2227–2242. https://doi.org/10.1007/s00170-017-1409-4
42. Insperger T, Stépán G, Turi J (2008) On the higher-order semi-discretizations for periodic delayed systems. J Sound Vib 313(1–2):334–341. https://doi.org/10.1016/j.jsv.2007.11.040
43. Guo Q, Sun YW, Jiang Y (2012) On the accurate calculation of milling stability limits using third-order full-discretization method. Int J Mach Tools Manuf 62:61–66. https://doi.org/10.1016/j.ijmachtools.2012.05.001
44. Liu YL, Zhang DH, Wu BH (2012) An efficient full-discretization method for prediction of milling stability. Int J Mach Tools Manuf 63:44–48. https://doi.org/10.1016/j.ijmachtools.2012.07.008
45. Farkas M (ed) (1994) Periodic motions. Springer-Verlag, New York
46. Ahmadi K, Ismail F (2012) Investigation of finite amplitude stability due to process damping in milling. Procedia CIRP 1:60–65. https://doi.org/10.1016/j.procir.2012.04.009
47. Elbestawi MA, Ismail F, Du R, Ullagaddi BC (1994) Modeling machining dynamics including damping in the tool-workpiece interface. J Eng Ind 116(4):435–439. https://doi.org/10.1115/1.2902125
48. Gradisek J, Kalveram M, Insperger T, Weinert K, Stepan G, Govekar E, Grabec I (2005) On stability prediction for milling. Int J Mach Tools Manuf 45(7–8):769–781. https://doi.org/10.1016/j.ijmachtools.2004.11.015
49. Ding Y (2011) milling dynamics-stability analysis methods and applications, Doctoral Dissertation, Shanghai Jiao Tong University
50. Long XH, Balachandran B (2010) Stability of up-milling and down-milling operations with variable spindle speed. J Vib Control 16(7–8):1151–1168. https://doi.org/10.1177/1077546309341131
51. Wang MH, Lei G, Zheng YH (2014) An examination of the fundamental mechanics of cutting force coefficients. Int J Mach Tools Manuf 78:1–7 https://doi.org/10.1016/j.ijmachtools.2013.10.008